The original journal article is available at `https://doi.org/10.1029/2018JC014341`.

Processing choices affect ocean mass estimates from GRACE

B. Uebbing[1], **J. Kusche**[1], **R. Rietbroek**[1], **F. W. Landerer**[2]

[1]Institute of Geodesy and Geoinformation, University of Bonn, D-53115 Bonn, Germany
[2]Jet Propulsion Laboratory, California Institute of Technology, Pasadena, CA 91109, USA

Key Points:

- Published ocean mass rates from GRACE differ by up to more than $1 mm/yr$ globally and for individual ocean basins
- The main reasons are (1) how different techniques correct for GIA, and (2) inconsistent restoring of the background atmosphere-ocean models
- We provide a reconciled range of ocean mass rates ($1.4 - 1.8 mm/s$ depending on analysis interval) that agrees within $0.1 mm/y$ across methods.

Corresponding author: Bernd Uebbing, uebbing@geod.uni-bonn.de

Abstract

Accurate estimates of ocean mass change are necessary to infer steric sea level change from sea level changes measured with satellite altimeters. Published studies using the GRACE satellite mission indicated a large range in trends (~1–2 mm/y) with reported standard errors of 0.1–0.3 mm/y. Here, we show that a large part of this discrepancy (up to 0.6 mm/y) can be explained by which model is used to account for the effect of glacial isostatic adjustment. The second-largest contribution (0.3–0.4 mm/y) is related to the way how different studies have restored atmospheric and oceanic signals which have been removed during the GRACE gravity estimation process. Here, two processing strategies, which previously resulted in differing ocean mass trends are considered. The 'direct' method uses the standard GRACE Stokes coefficients, while the 'inverse' method applies a joint inversion of data from GRACE and altimetry. After accounting for differences in processing corrections, global mean ocean mass estimates from the direct, the mascon and inverse approach agree with each other on global scales within less than 0.1 mm/y. Using the A et al. [2013] GIA model, we provide a reconciled monthly time series of global mean ocean mass, which suggests that ocean mass has increased by 1.43 mm/y over 2002.6–2014.5, with an amplified rate of 1.75 mm/y over 2002.6-2016.5 which covers almost the complete GRACE time span. However, we note that estimates as low as 1.05 mm/y cannot be ruled out when other published GIA corrections with lower mass-equivalent signals over Antarctica are used.

1 Introduction

Global mean sea level has risen by ~3.2 mm/y between 1993 and 2012 [*Church et al.*, 2013] and when accounting for volcanic eruptions, ENSO and decadal variability, the climate-change driven part of this observed rise is accelerating by 0.08 mm/y^2 [*Nerem et al.*, 2018]. However, developing and testing predictions for future sea levels requires a partitioning of the observed change into steric and mass components, the latter being related to ice sheet and glacier mass imbalance and changes in land water storage. Global and regional sea level budgets have been derived from various data sets [e.g. *Cazenave et al.*, 2009; *Dieng et al.*, 2015; *Rietbroek et al.*, 2016; *Chambers et al.*, 2017; *WCRP-Global-Sea-Level-Budget-Group*, 2018] but closing the sea level budget within a desired range of 0.1 mm/y represents still a challenge even at global scale.

While redistributions of mass between ocean basins reflect dynamic changes in ocean circulation e.g. caused by wind stress anomalies [*Boening et al.*, 2011; *Petrick et al.*, 2014], changes in total ocean mass are predominantly related to imbalances in the net freshwater flux from land and atmosphere, i.e. ocean evaporation, precipitation, global ice discharge and river runoff. In principle, three methods exist for deriving ocean mass change: (1) Altimetric observation of the total sea level change is corrected for steric (i.e. volumetric) sea level change from in-situ observations of temperature and salinity profiles and from modeling; (2) mass changes are directly obtained from GRACE satellite data products [e.g. *Johnson and Chambers*, 2013]; (3) GRACE mass observation and altimetric sea level observation are combined in an inverse approach [*Rietbroek et al.*, 2016] where one jointly solves for mass change and steric variations.

Long time series of altimetric observations with sufficient spatial and temporal coverage provide good estimates of global and regional sea level changes since the start of the Topex/Poseidon mission in 1993. While quasi-global steric sea level can be observed from Argo data since about 2005 for the upper 2000 m of the ocean, *von Schuckmann et al.* [2014] indicate an underestimation of the steric component due to insufficient spatial coverage from the available floats. Recent studies only consider the thermosteric sea level change and assume the halo-steric influence to be negligible in terms of its global average [*Nerem et al.*, 2018; *WCRP-Global-Sea-Level-Budget-Group*, 2018].

The Gravity Recovery and Climate Experiment (GRACE) mission has measured mass change in the Earth's water cycle between 2002 and 2017, and will be continued with the GRACE-FO mission [*Flechtner et al.*, 2016], launched successfully on May 22, 2018. Several authors have used Stokes coefficients, the standard level–2 GRACE data product, to derive ocean mass estimates. For processing the GRACE data directly [*Chambers and Bonin*, 2012; *Johnson and Chambers*, 2013] (denoted as the 'direct method') these spherical harmonic coefficients are combined with external corrections and an ocean kernel that minimizes land leakage by effectively shrinking the ocean area. This approach has led to ocean mass rates of, e.g., 2.0 mm/y over 2005-2013 [*Llovel et al.*, 2014], 1.9 mm/y over 2005-2014 [*Feng and Zhong*, 2015] or 2.1 mm/y over 2005-2015 [*Chambers et al.*, 2017]. At the time of writing, i.e. without GRACE and prior to the availability of GRACE-FO data, monthly spherical harmonic coefficients can be derived at much lower resolution from the Swarm satellite mission, which yield global ocean mass rates similar to GRACE in the overlap period but with higher uncertainties [*Lück et al.*, 2018]. Hydrological leakage arises from land water storage variations in coastal regions and biases ocean mass estimates by averaging a truncated spherical harmonic expansion. *Fenoglio-Marc et al.* [2006] tried to mitigate this by removing variations in total water storage from hydrological modeling beforehand. However, this could introduce potential non-physical trends from the hydrological models [*Scanlon et al.*, 2018]. It is more common to apply an additional buffer zone (usually about 300km) along the coasts in order to mitigate the hydrological leakage effect [*Johnson and Chambers*, 2013].

The difficulty in separating ice, ocean and land mass signals in the GRACE data has lead to the development of so-called inverse approaches. An early inverse approach by *Plag and Juettner* [2001] suggested that spatial patterns of sea level change observed with a global network of tide gauges might be inverted into fingerprints of ice mass change. *Jacob et al.* [2012] analysed GRACE spherical harmonics by fitting spatially distributed patterns of glacier ice melt. Also, *Chen et al.* [2013] derived ocean mass change by employing a forward modeling approach which allows to reconstruct mass rates for the ocean, polar ice-sheets, mountain glaciers and terrestrial water storage simultaneously. The core of the *Rietbroek et al.* [2016] (hereafter termed 'R16') method represents a solution to the inverse problem at GRACE and altimetry normal equation level, after reparameterization from Stokes coefficients to a lower-dimensional solution space. A fundamental difference to the direct approach is that this allows one to take into account the GRACE error structure, and that the method avoids external geocenter, GIA and leakage corrections in a preprocessing step. Individual estimates for mass loss of the Greenland and Antarctica ice-sheets fit well to independent observations. But, the R16 estimate suggests overall ocean mass rates much lower than found via the direct approach (Fig. 1), with the implication that the steric contribution from the inverse approach does not fit to Argo-based estimates, e.g. reported in [*Llovel et al.*, 2014].

While these differences are clearly larger than could be explained through the GRACE measurement uncertainty, so far it has been suspected that an accumulation of minor inconsistencies in the analysis of the GRACE level 2 data between the two approaches is responsible for them. Here, we focus on (1) differences in the interpretation of the monthly time-averaged ocean de-aliasing data products (AOD1B) [*Flechtner et al.*, 2015] provided by GFZ Potsdam and the Center for Space Research (CSR) of the University of Texas. These products are required to convert GRACE level–2 products into mass-driven sea level change for comparison with radar altimetry; (2) the different assumptions that underlie the correction of solid-Earth effects resulting from past deglaciation cycles in the direct and inverse approaches (i.e. the GIA correction).

In order to prevent tidal and non-tidal fast barotropic motions in atmosphere and ocean from aliasing into monthly and longer timescales, such signals are removed from GRACE data during the level–1 processing. In GRACE release 05, the 'background modeling' considers atmospheric mass redistribution derived from ECMWF surface pres-

sure, moisture and temperature fields, and ocean mass redistribution obtained from simulating with the Ocean Model for Circulation and Tides (OMCT) [*Thomas et al.*, 2001] consistently with ECMWF pressure and wind stress fields. At the level of monthly level–2 GRACE data, the so-called 'GAC-' or 'GAD-products' are then applied to restore the monthly mean of the 6-hourly ocean dealiasing background models. The resulting GRACE data will then contain the full ocean and atmosphere signal. The GAD product, in contrast to the GAC product, is based directly on surface pressure fields, and does not account for upper-air density anomalies [*Flechtner et al.*, 2015]. Moreover, altimetric sea level is usually corrected for sea surface pressure variations assuming a modified inverse barometric response. In order to properly assess the sea level budget, the GRACE and altimetry data have to be corrected for the atmospheric pressure effects in a consistent manner. To this end for GRACE, the GAD-product has been suggested to be further modified by removing its monthly ocean average, i.e. the ocean mean of its surface pressure component [*Johnson and Chambers*, 2013; *Feng and Zhong*, 2015]. However, as we will see later, this practice can lead to inconsistencies that may introduce surprisingly large artifact rates.

The GIA correction in GRACE analysis takes into account the ongoing redistribution of mantle material due to the viscoelastic response of the Earth to past deglaciation cycles. In the direct approach, this response is generally derived from a single run of a spectral or finite-element isostatic adjustment model forced by prescribed ice load history, with given viscosity profiles [e.g., *A et al.*, 2013]. GIA has no direct contribution in terms of global mean relative sea level, but it influences the estimates for the Antarctic mass loss contribution, and to a lesser extent, for Greenland and glaciers. It is common to subtract a GIA correction of approximately -0.3 mm/y from the altimetry record [*Douglas and Peltier*, 2002; *Nerem et al.*, 2010] to convert from global mean geocentric sea level to relative sea level. It is important to keep in mind that the GIA correction affects GRACE and altimetry in a different way, and that GRACE based estimates are much more sensitive to errors in the GIA model [*Tamisiea*, 2011].

Others have pointed out that these assumptions limit GRACE mass change estimates in particular for Antarctica [e.g., *van der Wal et al.*, 2015]. In the inverse approach for deriving ocean mass from GRACE and altimetry, individual patterns of gravitational response due to ice melt in Antarctica, Greenland, and land glaciers in combination with patterns accounting for terrestrial hydrology are empirically calibrated (i.e. scaled) to achieve the best fit to GRACE while at the same time the volumetric response of the same load histories is fitted to the altimetry data, together with all other known mass and steric patterns. As a result, the inverse approach generates a semi-empirical version of the GIA model that can differ significantly from the original (uncalibrated) model run [*Rietbroek et al.*, 2016]. Most notably, the estimated Antarctic GIA component from *Rietbroek et al.* [2016] was significantly smaller than the apriori 1D model which was based on ICE5G and VM2 [*Klemann and Martinec*, 2009]. Accordingly, such differences also propagate to ocean mass corrections. To establish a comparison framework with a common GIA correction, we will introduce an extension to the *Rietbroek et al.* [2016] methodology to make the inverse approach agree as much as possible with the direct approach, by constraining the GIA correction in the inverse procedure to a given model output.

This article is organized as follows: In section 2 we first provide information on the utilized data sets and how to derive ocean mass change from the direct and inverse approaches. In section 3 we review the direct and inverse methods for deriving ocean mass change from GRACE with respect to conceptual similarities and differences during processing. We focus on analysis options for correcting for GIA and restoring the atmosphere-ocean background models. Then in section 4 we evaluate various solutions, with the same data but by applying corrections as consistent as possible, with respect to the global ocean. Section 5 concludes our study and highlights how GIA and the GAC/GAD corrections affect the global ocean mass estimates.

2 Data and Methods

2.1 Direct Approach

In the direct method for estimating ocean mass change from GRACE we follow *Chambers and Bonin* [2012] and *Johnson and Chambers* [2013] (hereafter called 'JC13') and update it where necessary. First, one constructs a global surface mass change representation from the RL05 GRACE level-2 data GSM_{L2}, available from `ftp://podaac-ftp.jpl.nasa.gov/allData/grace/L2/`. For this study, we utilize the RL05 gravity fields from the University of Texas, Centre for Space Research (CSR) available up to degree and order 60 and the fields from Geoforschungszentrum (GFZ) available up to degree and order 90. Since GRACE does not provide the degree-1 coefficients that correspond to that part of the mass redistribution that can be expressed as a relocation of the center-of-mass, these have to be augmented with external information, such as, in this case, from *Swenson et al.* [2008]. Similar, the c_{20} coefficients are replaced by estimates obtained from satellite laser ranging and provided by *Cheng et al.* [2013], but we note that this does not properly account for error correlations [*Sun et al.*, 2016]. As an additional step for the RL05 processing (not required for RL06), we also apply the pole tide correction [*Wahr et al.*, 2015] which modifies the C_{21} and S_{21} coefficients. Note that this is not considered when strictly following the JC13 processing (see also Section 3.3).

For deriving mass changes, a mean field over the time period 2005–2010 is subtracted from each monthly gravity field. The GIA trends from *A et al.* [2013] are used to account for the GIA effect. At this point, it is possible to further smooth and/or decorrelate the GRACE data in order to average out correlated noise. However following *Chambers and Willis* [2009] and *Johnson and Chambers* [2013], we do not apply any filtering. Afterwards, Stokes coefficients are converted to equivalent water height (EWH). When strictly following the JC13 processing, one would then compute the final basin average up to degree and order 60 without any restoration of the AOD1B background model.

Here, we modified two aspects of the JC13 approach. Before computing the basin average over the ocean and after a potential filtering step [*Flechtner et al.*, 2015], the AOD1B background model has to be restored. For ocean applications, one utilizes the monthly mean GAD product. In order to derive ocean mass change and, at the same time, be consistent with the IB correction applied to altimetry, we remove the mean value over the total ocean from each monthly GAD field before adding it back to the spherical harmonics. In addition, we only considered the spherical harmonics up to degree and order 40, which is equal to filtering out all signals on spatial scales larger than ~1000 km. We refer to Sections 3.2 and 3.4 for details on how this modified IB correction and the truncation affects the JC13 processing.

Finally, the result of this procedure is convolved with an ocean kernel (unlike in altimetry, the ocean basin typically includes latitudes beyond 66°). To avoid contamination of the ocean signal from large-amplitude land water storage changes, one typically applies a buffering zone of a few hundred km around coastal areas effectively shrinking the ocean area to compute the final ocean average. In what follows, we assume this zone extends over 300 km (see also S2).

For comparison, we utilize the ocean mass time series derived from *Johnson and Chambers* [2013] which is publicly available from `https://dl.dropboxusercontent.com/u/31563267/ocean_mass_orig.txt` and has been used in several studies, e.g. [*Dieng et al.*, 2015; *Piecuch and Quinn*, 2016; *Chambers et al.*, 2017].

2.2 Inverse Approach

2.2.1 Method of Rietbroek et al. [2016]

In the inverse method proposed by *Rietbroek et al.* [2016], GRACE gravity data and Jason-1/-2 altimetry data are fitted to a set of predefined spatial patterns in order to estimate corresponding monthly scaling factors. These patterns, also termed 'fingerprints', are generally assumed as stationary, with the implication that propagating phenomena in sea level or mass change map may not be fully captured. R16 consider 119 mass patterns for melting contributions from the ice-sheets in Greenland and Antarctica, melting of land glaciers and changes in terrestrial hydrology. Including hydrological patterns, here derived from the WaterGAP Global Hydrological Model (WGHM) [*Döll et al.*, 2003; *Müller Schmied et al.*, 2014], enables us to explicitly account for leakage effects. Of course, this depends on how well the land patterns, which are obtained from EOF analysis applied to hydrological model output (2002–2010), describe reality. The passive sea level response from the mass related patterns is forward modeled utilizing the sea level equation [*Farrell and Clark*, 1976]. The 200 steric fingerprints are computed from monthly steric sea level variations derived from modeled temperature and salinity variations. For this, a principal component analysis is applied to the modeled steric data (1990–2011) from the Finite Element Sea Ice-Ocean Model (FESOM) [*Timmermann et al.*, 2009] and the 200 leading empirical orthogonal functions (EOF) are retained as fingerprints. To capture dynamical redistributions of ocean mass and remaining steric effects, a set of currently 100 auxiliary fingerprints [*Rietbroek et al.*, 2016] is derived from the residuals of the reconstructed total sea level with altimetry.

The GRACE input data are monthly Stokes coefficients in the form of unsolved GRACE normal equations systems, provided by GFZ up to degree and order 150. The normal equations, which are usually solved for the monthly GFZ level–2 spherical harmonic stokes coefficients, are reparameterized to lie in the solution space spanned by the spatial patterns which can be viewed as lumped spherical harmonics. Thus, they do not require additional smoothing. In this method, degree-1 coefficients and c_{20} do not have to be inserted from external data but are rather derived from the combination of GRACE and altimetry data in the inverse solution. The AOD1B background model is restored to the input GRACE normal equation systems to include the full ocean mass signal (see also Sect. 3.2).

Jason-1 and -2 altimetry 1Hz along-track altimetry data are extracted from the Radar Altimetry Database System (RADS) [*Scharroo et al.*, 2013], from which we compute fully corrected sea level anomalies (SLA). The SLAs represent information on the total sea level change, i.e. the sum of mass and steric related sea level changes, while GRACE can only measure mass changes within the ocean.

The inverse approach, then combines the GRACE and altimetry data on normal equation level by fitting monthly scaling factors for the individual spatial patterns. The addition theorem for normal equations is used to combine the monthly normal equations and the systems are weighted by utilizing variance component estimation [*Förstner*, 1979]. Multiplying individual patterns with the corresponding scaling factors and summing over groups of patterns allows to reconstruct the total sea level change, but also separate it into individual contributions. In this study, we focus on the mass contribution, i.e. the sum of the 119 (rescaled) mass patterns.

In the R16 inverse approach, a correction to a given GIA model [*Klemann and Martinec*, 2009] is co-estimated from the GRACE and altimetry data by fitting five GIA related patterns for each of the major GIA regions, which were kindly provided to us by V. Klemann. The complete modelled GIA signal is used as an a priori model, by propagating the model to along track geoid height changes, and potential anomalies, so the inversion estimate represents an update to it. The inverse GIA solution can be used in the direct

method for consistency and for isolating other effects. Similarly, we can derive the degree-1 coefficients from the R16 inverse method and subsequently introduce them in the direct solution [*Jensen et al.*, 2013; *Wu et al.*, 2017]. The degree-1 coefficients from the inversion have been compared by *Sun et al.* [2017] to other solutions and revealed a good agreement with *Swenson et al.* [2008]. More details on the inverse method can be found in S4 in the supplementary information and in *Rietbroek et al.* [2012], *Jensen et al.* [2013], *Rietbroek* [2014], *Kusche et al.* [2016], and *Rietbroek et al.* [2016].

2.2.2 Modifications to the Rietbroek et al. [2016] Method

To be as consistent as possible with the direct method, we modified the R16 inversion. For this, we applied the same correction of the background AOD1B model (GAD), consistent with Section 3.2. We constrained the estimation of the GIA correction to *A et al.* [2013] by fixing the estimated GIA parameters to be zero and corrected for the *Wahr et al.* [2015] pole tide effect, which has not been accounted for in R16. Furthermore, to better capture oceanic mass redistribution, we introduce an additional set of mass patterns corresponding to ocean bottom pressure (OBP) derived from the ORAP5 ocean reanalysis [*Zuo et al.*, 2017]. The OBP patterns are constrained to always have a zero mean over the full ocean area, but regional trend estimates may still be different from zero. Thus, the OBP patterns represent internal mass variations within the ocean. The applied corrections are summarized in Table S1 in the supplementary information.

2.3 Additional Data Sets

For an additional comparison, we computed ocean mass by subtracting steric sea level change from the total change measured by altimetry. The global mean altimetry data is based on a continuously updated time series derived from Topex/Poseidon, Jason-1, Jason-2 and Jason-3 data which is available from `http://sealevel.colorado.edu/` and also accounts for the GIA contribution. For the thermo steric data we utilized 4D temperature variations from the ORA-S4 reanalysis product [*Balmaseda et al.*, 2013], available from `ftp://ftp-icdc.cen.uni-hamburg.de/EASYInit/ORA-S4/`. These were converted to steric sea level change and averaged over the global ocean. Furthermore, we compare to an ocean mass time series derived from the JPL v02 mascon solution available at `http://grace.jpl.nasa.gov`, supported by the NASA MEaSUREs Program. Originally, the JPL v02 mascon product had the (unmodified, see Section 3.2) GAD product restored. But, in order to derive ocean mass comparable to our direct and inverse approaches we additionally remove the GAD mean over the total ocean for each month. Afterwards, the global ocean mass can be directly computed from an area-weighted average.

For investigating the effect of individual GIA models on the ocean mass estimate, we utilize model data from *Paulson et al.* [2007] which was widely used for processing GRACE data in the past and has nowadays been replaced by the model from *A et al.* [2013]. Both models are available from `ftp://podaac-ftp.jpl.nasa.gov/allData/tellus/L3/pgr/`. In addition we compare to the model by *Klemann and Martinec* [2009]. This model is also the basis for the R16 inversion. We also utilize high resolution Stokes coefficient trends from the ICE6G-C GIA model by *Peltier et al.* [2015] available from `http://www.atmosp.physics.utoronto.ca/~peltier/data.php`. Finally, we consider the recently published GIA model by *Caron et al.* [2018] who analyzed a total of 128.000 forward models, assuming a radially symmetric Earth, where we utilize the expectation value available from `https://vesl.jpl.nasa.gov/solid-earth/gia/`.

3 Effects of Processing Corrections on Ocean Mass Estimates

We investigate the differences in processing choices between the direct and inverse approaches and evaluate their impact on the final ocean mass estimate. For the direct method we started with the published GFZ and CSR ocean mass time series which we were able to reconstruct within about 0.05 mm/y (Fig. 1 and Table 1). For reconstruction of the JC13 estimates, we neither applied the *Wahr et al.* [2015] pole tide correction, nor did we apply the GAD correction. Small remaining differences are likely related to small differences in the applied ocean mask (see also S2), including a 300km coastal buffer, but are inconsequential to any of our conclusions. This represents the basis of our investigations in the following sub-sections.

In the following, all basin averages and trends that we report are referred to an ocean basin excluding a 300 km buffer zone, while the basin used for reducing the GAD ocean mean can have different buffer areas. For comparing trends, we will consider the time period 2005-2013 (as in *Llovel et al.* [2014]), 2002.6-2014.5 (as in *Rietbroek et al.* [2016]) and almost the full available GRACE period 2002.6-2016.5. We do not provide inversion results for the latter period since not all datasets are currently available.

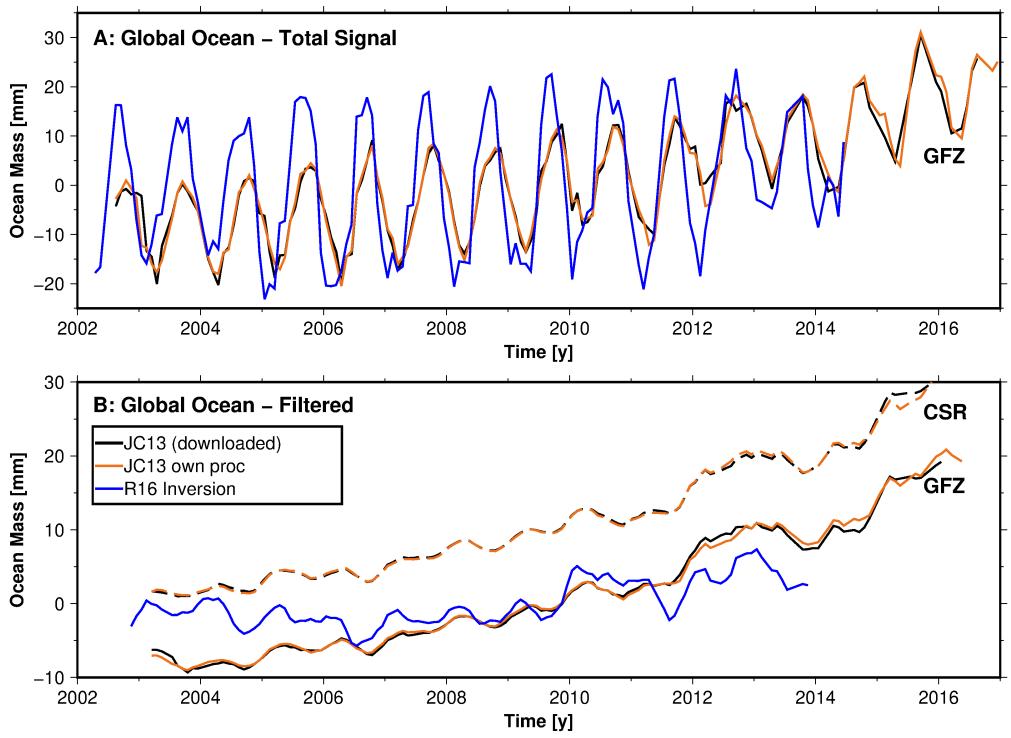

Figure 1. Global mean ocean mass time series from direct and inverse approaches. (A) Total global ocean mass signal. (B) Filtered with a 13 month boxcar filter. The CSR results are offset for clarity. The first and the last six month of each curve are affected by filter cutoff effects and have been omitted.

3.1 The GIA Correction

Glacial Isostatic Adjustment (GIA) is the visco-elastic response of the Earth's surface to ice mass load from a past glacial maximum. We find that by far the largest contribution of about 0.67 mm/y EWH to the difference between the direct and inverse methods is due to the difference in the applied GIA corrections (Fig. 2, (A)). Since EWH is computed assuming an elastic Earth, the GIA values reported in Table 2 are not physi-

Table 1. Previously published ocean mass trends with their reproduced versions. Note that the reconciled estimates are provided in Table 4. The trends are derived from the direct and inverse methods, as well as from the difference between altimetry and steric sea level. All trends are computed as mean equivalent water height (EWH) over the full ocean exclusive a 300 km buffer zone along the coasts (see S2 in supplementary material). No additional smoothing has been applied.

Source	2002.6-2014.5 $[\frac{mm}{y}]$	2005.0-2013.9 $[\frac{mm}{y}]$	2002.6-2016.5 $[\frac{mm}{y}]$
Johnson and Chambers [2013] CSR, (downloaded)	1.812	2.006	2.123
Johnson and Chambers [2013] GFZ, (downloaded)	1.747	2.078	2.007
Own proc. *Johnson and Chambers* [2013] (300 km GAD) CSR	1.829	2.029	2.164
Own proc. *Johnson and Chambers* [2013] (300 km GAD) GFZ	1.772	2.034	2.081
Rietbroek et al. [2016]	0.792	1.057	-

cally meaningful and represent an 'apparent mass change' [*Chao*, 2016]. However, they provide an order of magnitude for the effect of correctly applying the GIA correction, and differences point at possible errors in ocean mass trend estimates. While the empirically adjusted estimate in *Rietbroek et al.* [2016] corresponds to only -0.5 mm/y EWH, the constrained GIA correction from *A et al.* [2013] corresponds to -1.17 mm/y. Trends from other GIA models deviate by about 0.2 mm/y from the *A et al.* [2013] model, except for the GIA correction derived from *Klemann and Martinec* [2009] (-0.78 mm/y). Since the GIA correction is a strictly linear trend correction, amplitudes and phases will not be modified by this correction.

Table 2. Effect on global ocean mass of applying different GIA model corrections. All trends are computed as mean equivalent water height (EWH) over the full ocean exclusive a 300 km buffer zone along the coasts (see S2 in supplementary material). No additional smoothing has been applied. $\Delta\text{GIA}^{\textit{Rietbroek et al.}\ [2016]}_{\textit{A et al.}\ [2013]}$ represents the difference between the GIA trends from *Rietbroek et al.* [2016] and *A et al.* [2013]. All GIA trends reported here in EWH represent 'apparent mass change'.

Source	2002.6-2014.5 $[\frac{mm}{y}]$	2005.0-2013.9 $[\frac{mm}{y}]$	2002.6-2016.5 $[\frac{mm}{y}]$
Rietbroek et al. [2016] + $\Delta\text{GIA}^{\textit{Rietbroek et al.}\ [2016]}_{\textit{A et al.}\ [2013]}$	1.458	1.723	-
GIA *A et al.* [2013]		-1.166	
GIA ICE6G *Peltier et al.* [2015]		-1.145	
GIA *Paulson et al.* [2007]		-1.244	
GIA *Caron et al.* [2018]		-1.322	
GIA *Klemann and Martinec* [2009]		-0.783	
GIA *Rietbroek et al.* [2016]		-0.500	

When the trend difference $\Delta\text{GIA}^{\textit{Rietbroek et al.}\ [2016]}_{\textit{A et al.}\ [2013]} = 0.66 mm/y$ between the GIA corrections from *A et al.* [2013] and the *Rietbroek et al.* [2016] inversion is accounted for, the R16 inversion results agree well with the estimates based on the *A et al.* [2013] GIA correction (compare Table 3 and 4). The difference is mainly due to the significant down-

scaling of the Antarctic GIA component during the *Rietbroek et al.* [2016] inversion. Although the downscaling of the Antarctic component is consistent with the findings by independent studies [*Whitehouse et al.*, 2012; *van der Wal et al.*, 2015; *Martín-Español et al.*, 2016; *Barletta et al.*, 2018] in terms of geoid and uplift height, we do note that the resulting change, in terms of apparent mass change (-0.5 mm/yr), is very low compared to other GIA estimates. Discussing the GIA modeling in more detail is out of the scope of this study, but it becomes clear that correctly accounting for GIA has a very significant effect on deriving ocean mass estimates of direct and inverse approaches alike. We emphasize that resolving the uncertainties of the GIA signals in Antarctica are therefore key to increasing the acurracy of the sea level budget, but also related fields such as hydrology.

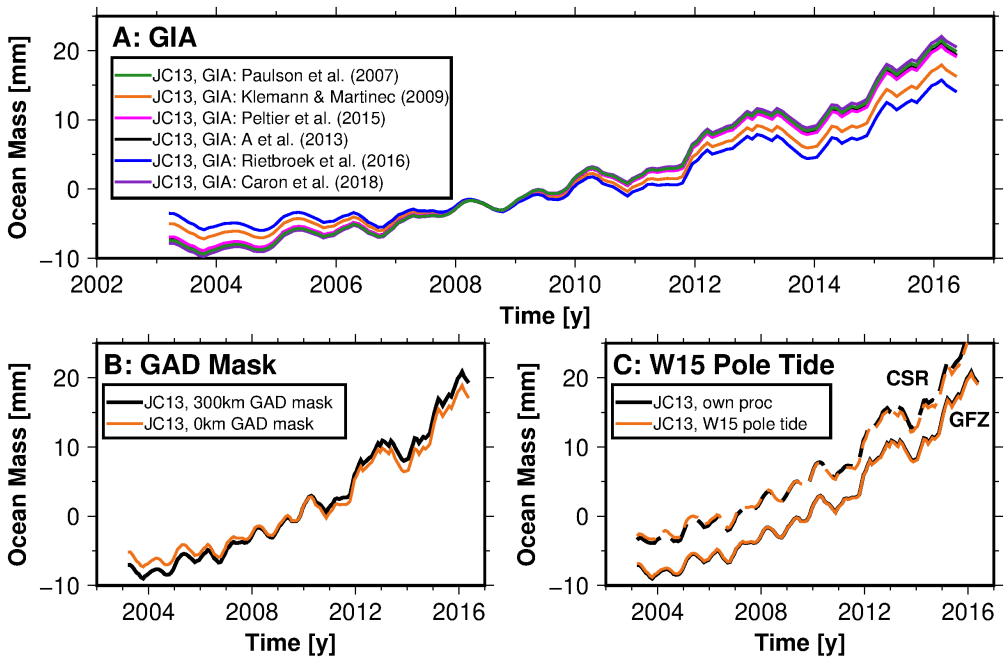

Figure 2. Effects of individual processing choices on the global ocean mass time series. (A) The effect of applying different GIA corrections (note that the R16-GIA has been extracted from the results of *Rietbroek et al.* [2016] and is applied here within the direct method). (B) The effect of utilizing a 300km coastal buffer zone or a 0 km coastal buffer zone for computing the GAD ocean mean. (C) The effect of the *Wahr et al.* [2015] pole tide (W15 PT) correction. The results for (A) and (B) are based on GFZ data only, since after applying the correction from (C) the resulting time series from both processing centers agree well. The first and the last six month are affected by filter cutoff effects and have been omitted here.

3.2 Restoring the AOD1B Background Model

During GRACE level-1 processing, the effects of ocean and atmosphere mass redistribution are removed prior to accumulating and solving monthly normal equations. To this end, model simulations are used that not necessarily represent best estimates at all time scales or for all ocean basins. For ocean applications, the monthly average of these simulations has to be restored to GRACE level-2 data prior to further analysis. This applies in the same way to direct and inverse estimates of ocean mass. However, it has been suggested to modify these monthly averages further to render them consistent with the way how the modified inverse barometric correction is applied in altimetry. This is where inconsistencies can have a significant effect on ocean mass change estimates.

The GRACE mission measures the total mass signal, i.e. the full effect of atmospheric and oceanic mass redistribution. Over the ocean, this total signal can be compared to ocean bottom pressure (OBP) recordings [*Dobslaw et al.*, 2013]. For the RL05 processing, the individual processing centers reduce the modeled atmospheric and oceanic mass contributions with a temporal resolution of 6 hours (3 hours for RL06). Consequently, the monthly L2 gravity fields are provided relative to these background models. In order to enable users to restore the removed signals, the processing centers provide the monthly mean fields of the atmospheric, i.e. the GAA product (for the RL05 data the ECMWF operational analysis fields at various vertical pressure levels are used, to derive the gravitational effect of dry and moist air via 3D integration), and the modeled ocean component, i.e. the GAB product (OMCT model) [*Flechtner et al.*, 2015]. In addition, two more products are provided. The GAC product represents the full effect that has been removed during level–1 processing, i.e. the sum of the GAA and GAB products. The GAD product is used for adding back the OBP component of the background models. It is only defined over the ocean and includes the GAB product, but only the surface pressure component of the GAA product without the upper-air density anomalies [*Flechtner et al.*, 2015]. No formal errors are provided for these products, but model imperfections still cause errors in these products.

When deriving OBP, one has to restore the oceanic component and atmospheric pressure acting on the sea surface, but not the upper-air density anomalies. Consequently the GAD product is restored by

$$OBP = GSM + GAD. \tag{1}$$

Here, we define GSM as the original data, GSM_{L2}, processed as described above with a mean field reduced and with all corrections for degree 1, c_{20}, pole tide (for RL05), and GIA applied. Restoring the GAC product at this point would also include the small upper air density anomalies which will influence the resulting trend value in the order of less than 0.1 mm/y. The OBP derived by Eq. (1) is comparable to measurements from OBP recorders. But, it does not represent the ocean mass component context of sea level budgets in combination with satellite altimetry.

During the processing of satellite altimetry the range measurements have been corrected for the inverse barometric (IB) effect. The inverse barometric correction applied to altimetry assumes that the ocean reacts to surface pressure variations but cannot react to net (spatially averaged) surface pressure change; this is the so-called 'modified IB correction' (MIB). In practice, it is almost always assumed to be the total ocean area [*Andersen and Scharroo*, 2011] although this is not necessarily true in reality [*Ponte*, 2006; *Mathers and Woodworth*, 2006].

In order to make the GRACE data consistent with altimetry and the applied MIB correction, it is necessary to remove the surface pressure component (here denoted as $\widehat{GAA}$; note that this product is not available to the user) after restoring the GAD product by

$$OcM = GSM + GAD - \left[\widehat{GAA}\right]_{mib}. \tag{2}$$

In the above, $[x]_{mib}$ means the spatial average of quantity x over the domain where, in the processing of radar altimetry, we assume that the average pressure cannot act on the ocean because of limited seawater compressibility. Since the surface pressure component $\widehat{GAA}$ is not provided as an individual product, it was suggested to modify the GAD product by removing its mean over the ocean [*Chambers and Bonin*, 2012; *Feng and Zhong*, 2015]. Here, we also remove the GAD ocean mean. However, the GAD product is defined as the sum of GAB and $\widehat{GAA}$. Consequently, this necessitates that the global mean of the ocean simulation (the GAB product) is zero at every time step. This is indeed enforced by keeping the total ocean mass constant at any time-step of the OMCT model run. After computing anomalies by removing a temporal average, the global mean over the total ocean is in fact zero [*Flechtner et al.*, 2015]. As a result, any deviations from zero for the

ocean mean value can be attributed to the atmospheric surface pressure component in the GAD product. This can be exploited to construct an MIB-like correction to GRACE, by removing the global ocean mean. The resulting MIB-corrected GRACE data then provides an ocean mass (OcM) signal consistent with the MIB-corrected altimetry and Eq. (2) can be written as

$$OcM = GSM + GAD - [GAD]_{mib}\,. \tag{3}$$

All these computations include the degree 0 and degree 1 coefficients. Since the degree 1 coefficients from *Swenson et al.* [2008] are estimated relative to the AOD1B background models, we add back the degree 1 coefficients from the GAD fields to include the full effect. In case one applies other degree-1 coefficients which include the full signal, obviously, the degree 1 GAD coefficients should be ignored. In addition, we also account for the degree 0 coefficients of the GAD product. The GAD product is derived by applying a masking operation in order to set the values to zero over land. This effectively removes mass which is then represented in the degree 0 coefficients and, consequently, should be properly accounted for. While this has no effect on ocean mass estimates, since the degree 0 adds a constant value which is then, again, removed by computing the corresponding ocean mean (see Eq. (3)). It will affect the estimation of OBP in the order of about 0.03 mm/y.

As a consequence, the time series of the monthly averaged ocean simulation with the OMCT model, that was removed from GRACE during level–1 processing, has a zero trend by definition but this is true only over the full ocean. It also means that trends for regional ocean basins or masked versions of the ocean average have non-vanishing trends that do not reflect reality [*Flechtner et al.*, 2015; *Dobslaw et al.*, 2013]; this applies in particular in shelf zones.

After restoring the GAD product either for deriving OBP (Eq. (1)) or OcM (Eq. (3)) it is possible to derive basin averages for a sub-region of interest to compute a time series of OBP or OcM. The region-averaged ocean mass signal β_{reg} is then

$$\beta_{reg}^{OBP} = [OBP]_{reg} = [GSM + GAD]_{reg}\,, \tag{4}$$

and

$$\beta_{reg}^{OcM} = [OcM]_{reg} = [GSM + GAD - [GAD]_{mib}]_{reg}\,. \tag{5}$$

Eq. (5) can be further separated as

$$\beta_{reg}^{OcM} = [OcM]_{reg} = [GSM + GAD]_{reg} - [GAD]_{mib}\,, \tag{6}$$

under the assumption that our averaging operator over an arbitrary region conserves the value of a uniform layer

$$[c]_{reg} = c. \tag{7}$$

It is important to note that the basin utilized for deriving the GAD-correction, i.e. $[GAD]_{mib}$, should in general be equal to the total ocean area. Employing the same basin to the GAD computation as for the final basin average will significantly affect the resulting OcM time series. For deriving OcM, this has given rise for some inconsistencies. In more detail, we have seen two procedures:

1. One uses the full ocean basin right up to the coast (see Figure S2 in the supplementary material) in removing the monthly mean GAD product – this means using $[GAD]_{mib} = [GAD]_{oc}$, where the subscript 'oc' indicates the total ocean.
2. One uses the same basin function that is employed later for computing the mean for a specific region, e.g. the full ocean minus a 300 km coastal buffer to account for leakage from land hydrology (see Figure S2 in the supplementary material), for computing the GAD monthly mean. Continuing this reasoning one could chose any ocean basin smaller than the full ocean. This would basically compute OBP

variations inside the basin but not with respect to global variations. In other words, one assumes $[GAD]_{mib} = [GAD]_{reg}$. In case the basin chosen for computing the mean GAD value would perfectly match the basin used for deriving the final basin average, this would be equivalent to not restoring the GAD product at all.

Computing the total ocean mean as suggested in procedure (1) appears to be correct since it will, theoretically, restore the same signal that has been removed before, i.e. during the estimation of the GRACE coefficients and lead to consistency with the altimetry MIB correction. However, if one is just interested in a smaller sub-basin (e.g. the ocean without the 300 km buffer), this procedure will introduce (or rather restore) significant trends from the GAD product for the computation of the basin average (here: $\sim$ 0.3-0.4 mm/y, see Table 3).

Following procedure (2) the GAD correction at the level–2 monthly data level will not add any additional trend to the basin considered for averaging the ocean mass, leaving only high frequency spatial patterns to be restored. The correction will be different for each basin and it will be difficult to make it consistent with altimetry, unless the MIB-correction for altimetry is indeed derived on basin scale. Moreover, (possibly non-physical) trends have been present in the AOD1B data that were removed during level–1 processing, especially in the coastal shelf zones [*Dobslaw et al.*, 2013]. It is difficult to argue they should not be restored. In addition, nearly all available altimetry products apply the MIB-correction computed with the global ocean mean of the surface pressure removed [*Andersen and Scharroo*, 2011], which supports the application of procedure (1).

Table 3. Direct GRACE estimates of ocean mass trends over the total ocean with coastal zones masked, but now with a GAD correction which accounts for the modified IB effect over the entire ocean (0km GAD). The last three rows indicate the trend effects in case the shallow ocean regions are masked when computing the GAD ocean average.

Source	2002.6-2014.5 $[\frac{mm}{y}]$	2005.0-2013.9 $[\frac{mm}{y}]$	2002.6-2016.5 $[\frac{mm}{y}]$
JC13, 0 km GAD, CSR	1.517	1.715	1.866
JC13, 0 km GAD, GFZ	1.459	1.720	1.782
GAD degree 0-100 CSR, 300 km buffer zone	-0.391	-0.402	-0.412
GAD degree 1-1 CSR, 300 km buffer zone	-0.105	-0.112	-0.102
GAD degree 0-100 CSR, 0 km buffer zone	-0.005	-0.014	-0.043

Computing the GAD ocean mean over an ocean basin exclusive a 300km coastal buffer zone results in ocean mass trends which are generally about 0.4 mm/y larger compared to computing the GAD ocean mean over the full ocean, i.e. a 0km buffer zone (Fig. 2, (B) and Table 3). About 25% of this effect is due to the degree 1 coefficients. Consequently, we suggest that deriving the GAD correction following procedure (1) yields an ocean mass time series which is more consistent with altimetry compared to procedure (2). The effect of applying procedure (1) instead of (2) has minor effects on the annual amplitude in the order of 0.3 mm reducing it by about 3%. We find less than one day for the annual and about 2 days for the semi-annual phase shift.

In order to reproduce the external ocean mass time series provided by *Johnson and Chambers* [2013] within a range of less than 0.05 mm/y one has to follow procedure (2) for restoring the AOD1B background model (Fig. 1). But as we have shown here, there is in fact a significant drift of shallow-region ocean mass with respect to deep-ocean re-

gions. Following procedure (1) and utilizing the total ocean basin for deriving the GAD correction leads to significantly smaller trends. For the direct method, the trends are now closer to what we find from the independently derived trends from subtracting steric sea level change from altimetry and the mascon solution (Tab. 4).

In *Rietbroek et al.* [2016], the GAC product is applied to the GRACE level–2 data (i.e. normal equations) instead of the GAD product. Only the mean value of the GAC product over the ocean was restored such that all computations were relative to a (reduced) background model $\widetilde{GAC} = GAC - [GAC]_{oc}$, i.e. GAC minus the total ocean mean of GAC. Since the utilized GRACE level–2 data already have the full GAC signal removed, the procedure can be summarized as

$$GSM_{inv} = GSM + [GAC]_{oc} \, . \tag{8}$$

In order to make the altimetry sea level anomaly (SLA) data consistent with the GRACE data corrected as described, the same background model ($\widetilde{GAC}$) has to be removed from the altimetry data

$$SLA_{inv} = SLA - (GAC - [GAC]_{oc}). \tag{9}$$

Consequently, one has to add back the background model ($\widetilde{GAC}$) after the inversion run in order to arrive at an estimate comparable to other solutions. *Rietbroek et al.* [2016] assumed that performing the estimation relative to the $\widetilde{GAC}$ background model would lead to reduced residuals. At the same time this also means that the modeled OBP signal is removed from the data before running the inversion with only a residual OBP signal left.

For the additional inversion run, which is consistent with the direct estimate, the AOD1B background model is restored in the same way as already described in Eq. (3), utilizing the GAD product. Therefore, no additional correction is required to the altimetry SLA. Restoring the background model this way, means that we now include the modeled OBP signal into our data sets and we therefore account for it by introducing the additional spatial patterns based on modeled OBP from the ORAP5 model. Both inversion runs, therefore, restore the AOD1B product according to procedure (1). Replacing the GAC product with the GAD product for the inversion method leads to slightly smaller residuals.

3.3 *Wahr et al.* [2015] Pole Tide Correction

The pole tide is caused by the Earth and oceans reacting to changes in polar motion which leads to gravity signals that predominantly affect the coefficients C_{21} and S_{21}. While the pole tide effect is usually removed by the processing centers, the removal of the mean pole has been handled in a different way in each of the centers for the RL05 processing. This resulted in different parts of the pole tide effect to still be present in the GRACE level–2 data [*Wahr et al.*, 2015]. Consequently, this has to be corrected when dealing with RL05 data. For the RL06 processing, the mean pole time series is derived in the same way for all processing centers according to a new linear model in the updated IERS conventions. Consequently, a pole tide correction is no longer necessary for RL06 data.

When comparing the RL05 trends for the two processing centers, we generally find trends smaller by about 0.1 mm/y from the GFZ solution compared to the CSR solution (see Table 1 and Fig. 1). The difference between the processing centers becomes smaller after accounting for the *Wahr et al.* [2015] pole tide correction. The correction depends on the processing center and the time period. For GFZ data we find it to be in the order of ∼0.03 mm/y and for CSR it is slightly larger in the order of ∼0.1 mm/y. The reason

is that the mean polar motion has been accounted for in a different way for both processing centers [*Wahr et al.*, 2015]. The effect on the (semi-)annual amplitude and phase from this correction is insignificant as this is mostly a trend correction. The *Wahr et al.* [2015] pole tide correction is neither considered when strictly following the JC13 processing, nor for the R16 inverse approach. We account for this effect in Section 4 in both approaches. Since the trend estimates of CSR and GFZ based time series agree well after this correction has been applied (Fig. 2, (C)), we will focus on the GFZ based time series in the following.

3.4 Corrections of Minor Influence

When strictly following the JC13 processing, one would have to utilize the unfiltered GRACE Stokes coefficients up to degree and order 60. This leads to significant aliasing effects (north-south stripes) in the data for higher degrees and orders. Generally it has been assumed that these stripes average out over the total ocean. However, we found that the trends derived from unfiltered data up to degree and order 60 to be more sensitive to small changes in the ocean mask, leading to trend differences of up to 0.1 mm/y (see also S2 in the supplementary information). To mitigate this, it is possible to either introduce a filtering step into the processing chain or to limit the maximum degree of the GRACE coefficients. For example, after applying a DDK5 filter [*Kusche*, 2007] to the JC13 processed data up to degree and order 60 and accounting for the filter-leakage effect we also derived a trend of 1.410 mm/y which agrees well to the corresponding trends reported in Table 4. On the other hand, limiting the maximum degree and order to 40 leads to a reduced spatial resolution of about 1000 km, but also leads to significantly weaker striping effects. The trends are then relatively robust with respect to small differences in the ocean mask (see also S2 in the supplementary information). Therefore in this study, we chose to utilize the unfiltered data only up to degree and order 40.

While the geocenter effect (~0.17 mm/y) on the total ocean mass trend is non negligible, the degree 1 estimates from *Swenson et al.* [2008] and *Rietbroek et al.* [2016] agree well within 0.01 mm/y. The trends from GAD-CSR shown in Table 3 agree within a range of 0.005 mm/y with the corresponding trends from GAD-GFZ (not shown). The reason for these minor differences is that for the generation of the monthly level–2 gravity fields, CSR and GFZ utilize data from different days during some of the months. Consequently, the corresponding GAD products, which always include full days of data used [*Flechtner et al.*, 2015], are produced to be consistent with the days utilized during the processing centers level–2 gravity estimation.

4 Reconciling Global Ocean Mass Estimates

On a global scale, we first compare the ocean mass time series from the direct method derived according to our descriptions in Section 2.1, the consistent inverse method (Section 2.2.2), the JPL mascon v02 solution and from subtracting steric sea level change from the ORA-S4 reanalysis from the total sea level change from altimetry (Section 2.3). Hereafter, the latter will be termed 'AltSter approach'. After correctly applying the GAD and pole tide corrections to the direct method, the trends of global ocean mass change agree well between the time series derived from CSR and GFZ data (Table 4). In addition, we find good agreement with the consistent inversion run and the ocean mass derived from altimetry and steric data (Table 4). For the mascon solution, the ocean mass trend is about 0.05–0.1 mm/y smaller compared to the direct and inverse approaches. To create a fully consistent mass time series, we would have had to repeat the mascon processing from level-1B data. Nevertheless, we have chosen to show the JPL v02 solution for the sake of comparison.

We find annual amplitudes of 11mm for the mascon, the direct and the inverse approach, while the amplitude from the AltSter approach is slightly smaller (8mm). Sim-

Table 4. Global ocean mass trends from direct and inverse approaches, as well as from subtracting steric sea level change from altimetry. All trends are computed as mean equivalent water height (EWH) over the full ocean exclusive a 300 km buffer zone along the coasts (see S2 in supplementary material). No additional smoothing has been applied.

Source	2002.6-2014.5 $[\frac{mm}{y}]$	2005.0-2013.9 $[\frac{mm}{y}]$	2002.6-2016.5 $[\frac{mm}{y}]$
JC13 (0km GAD; *A et al.* [2013] GIA; W15 PT), CSR	1.403	1.590	1.747
JC13 (0km GAD; *A et al.* [2013] GIA; W15 PT), GFZ	1.426	1.688	1.750
Inversion, (0km GAD; *A et al.* [2013] GIA; W15 PT)	1.432	1.682	-
Altimetry – (thermo-) steric	1.458	1.406	1.868
JPL Mascon v02	1.400	1.639	1.650

ilar, we find only small phase differences of a few days between the direct, inverse and mascon approach (277 days, 274 days, and 278 days, respectively) and a slightly larger phase offset for the AltSter approach (288 days). For the semi-annual amplitude we find differences of 0.3mm between the direct and inverse approach (0.4mm and 0.7mm, respectively), but only 0.1mm difference between the inverse and AltSter approach. For the mascon solution we find the semi-annual amplitude (0.5mm) to be close to the direct approach. We find a semi-annual phase offsets of 31 and 38 days for the direct and mascon method,respectively, while the inverse and AltSter method indicate offsets of 51 days and 65 days, respectively. The four methods are able to capture the annual cycle with similar accuracy but disagree slightly stronger on semi-annual and higher frequency time scales (see also Fig. 3, (A)).

Our ocean mass trends agree well between the individual methods, although we find smaller trends compared to published estimates [*Llovel et al.*, 2014; *Dieng et al.*, 2015; *Piecuch and Quinn*, 2016; *Chambers et al.*, 2017]. For example, *Chambers et al.* [2017] derived an ocean mass trend of 2.1 mm/y over the period 2005-2015 while we find a significantly smaller trend of 1.7 mm/y over the same period. As explained in this paper, the differences can be explained by the procedure of restoring the AOD1B product and accounting for the *Wahr et al.* [2015] pole tide correction.

A closer look at the individual time series (Fig. 3) reveals that there are still significant differences between the four approaches during some months; especially, after 2010. We note here that during the years 2009-2010 there was an extraordinary strong El Niño event followed by a strong La Niña event [*Kim et al.*, 2011]. Similar, we also find larger disagreement with the mascon approach after 2014 leading to a generally smaller ocean mass estimate compared to the direct approach (Fig. 3, (B)). The differences of the AltSter method (Fig. 3, (B) green) are larger with respect to the direct and inverse approaches (Fig. 3, (B) orange and cyan). This is related to the way the estimate is derived from the AltSter approach. Variations in the global altimetry time series and the ORA-S4 reanalysis directly translate into the derived ocean mass time series.

The inverse method (Fig. 3, (B) cyan) agrees well with the direct method before 2010 and the differences increase during the El Niño event. During 2012 it agrees with the direct and mascon solution. It is challenging to attribute these differences, because the methods are not mathematically equivalent. They do not use exactly the same data, and they do not involve the same physics (e.g., accounting for self-gravitation). Furthermore,

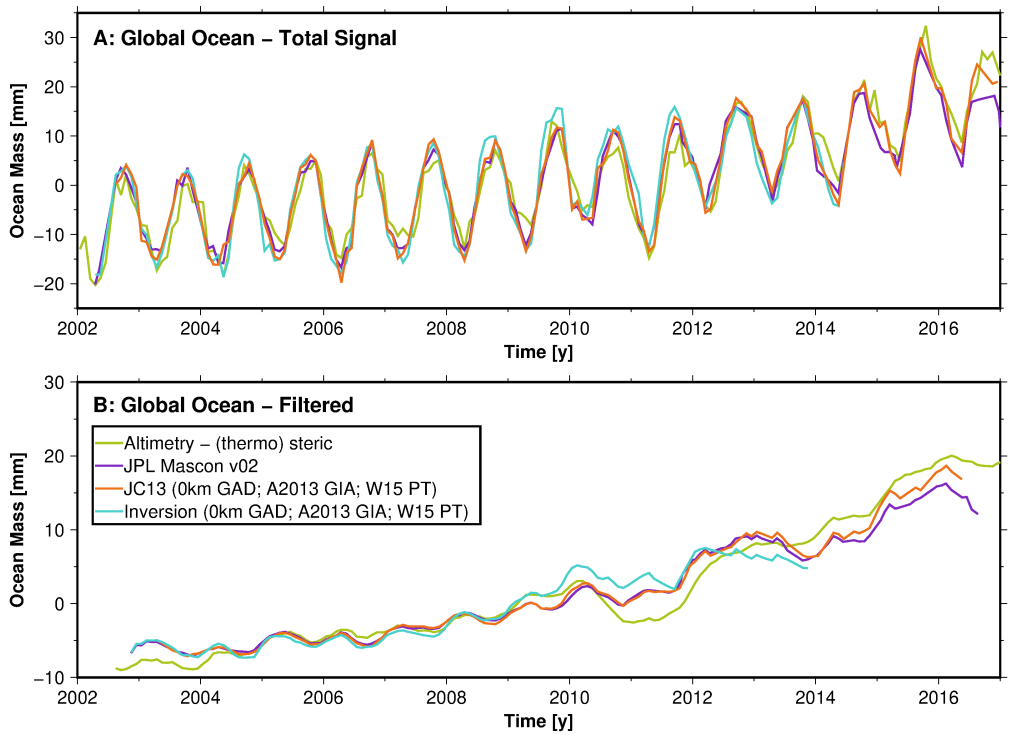

Figure 3. Global mean ocean mass time series from direct and AltSter approaches. (A) Total global ocean mass signal. (B) Filtered with a 13 month boxcar filter. All GRACE results refer to GFZ solutions. The first and the last six month of each curve are affected by filter cutoff effects and have been omitted.

the inverse approach utilizes the full covariance information, the data are weighted differently compared to the direct approach.

We hypothesize that the inverse method may not be fully robust with respect to the choice of patterns. Co-estimating the steric sea level change in the inverse approach from the combination of GRACE and altimetry has been shown to have only a small effect on the ocean mass estimates [*Kusche et al.*, 2016]. But, the reconstruction strongly depends on whether these patterns in combination with the estimated scaling factors are sufficient to reconstruct the ocean mass changes. Furthermore, the hydrological and steric patterns within the inversion are derived from model data over a limited time period (2002–2010 and 1990–2011, respectively). It is implicitly assumed that the EOFs derived from this period are still representative outside of the time period and can be used to partition the total sea level change. The larger differences after 2010 might thus be an indication that the assumption might be violated, especially for the steric patterns which capture a significant amount of spatial and temporal variability. However, first experiments with an extended time series (not shown here) indicate good correspondence with the direct and mascon approaches after 2014.

Yet, in case the EOFs from the model period are not able to correctly represent the variations after 2010, this will affect the reconstructions from the corresponding spatial patterns in the inversion. As a result, the mass estimates might be affected through the combined estimation of the mass and steric component within the inversion; the sum of the mass and the steric component is supposed to be equal to the total sea level measured by altimetry. Thus, improving the spatial patterns within the inverse approach, e.g. to better capture the representation of the El Niño/La Niña event by employing updated model data, may improve the estimated ocean mass component during these years. On the other

hand, in April 2011, the quality of the GRACE data notably degraded due to turning off the thermal stabilization of the on-board accelerometers [*Klinger and Mayer-Gürr*, 2016]. This had prompted changes in gravity processing strategies and increased the spread between different GRACE solutions.

5 Conclusions

Direct and inverse methods for deriving ocean mass estimates from GRACE only and in combination with altimetry have been compared. We find that published differences between the direct and inverse approaches can be explained by the handling of the GIA correction and restoring the AOD1B product. After adjusting for inconsistencies in the corrections, agreement in ocean mass estimates with the direct approach [*Johnson and Chambers*, 2013] is better than 0.1 mm/y for the global ocean. As a result for the period 2002.6 till 2014.5, we find the global ocean mass trend to be 1.43 mm/y from both approaches, when assuming that the *A et al.* [2013] GIA model is correct. We hypothesize that the global parameterization of the mass and steric components in the inverse approach may need to be improved to better account for the changes after 2010. To this end, future efforts will focus on augmenting the set of fingerprints with patterns derived from improved hydrological and ocean model runs which also cover a longer time span than the current model data. With contemporary GRACE and altimetry data, GIA is not well-constrained over Antarctica [e.g. *Martín-Español et al.*, 2016] and the implications of this discrepancy require further research. Consequently, the uncertainty related to this translates directly into estimates of ocean mass. The implication of our results is that steric sea level and ocean heat change over the GRACE era is probably at the higher end of the published range of estimates [e.g., *Nerem et al.*, 2018; *WCRP-Global-Sea-Level-Budget-Group*, 2018; *Resplandy et al.*, 2018].

In order to derive ocean mass estimates consistent with the inverse barometric correction applied in satellite altimetry, one needs to remove the average over the full ocean basin for each month. Neglecting the 300km coastal zone when restoring the GAD signal, as is done in several studies, then leads to inconsistencies which will affect the trend estimate in the order of 0.3 to 0.4 mm/y. Therefore, we suggest to apply the GAD correction as stated in procedure (1), described in Section 3.2. As a result, the ocean mass estimates are more consistent with satellite altimetry. It is important to note that while our study focused on the AOD1B models from release 05 of the GRACE data the same applies to the recent release 06 data. A first test with the already available RL06 GAD product and RL06 CSR data revealed that following procedure (2) would lead to a trend difference with respect to RL05 (for the period 2005.0 - 2013.99) of about 0.2 mm/y while the agreement was in the order of less than 0.05 mm/y after following procedure (1), again, supporting our suggestion for restoring the AOD1B product.

Acknowledgments
The ocean mass time series based on the direct and inverse approach can readily be downloaded from `https://www.apmg.uni-bonn.de/en/groups/apmg/data_and_models/time_series_of_ocean_mass_change_from_grace`. We acknowledge financial support by DFG (Grants KU 1207/22-1, OMCG) from the Deutsche Forschungsgemeinschaft (DFG) as part of the Special Priority Program (SPP)-1889 "Regional Sea Level Change and Society" (www.spp-sealevel.de). The work of F.W. Landerer was carried out at the Jet Propulsion Laboratory, California Institute of Technology, under a contract with NASA. We thank the editor Don Chambers and three anonymous reviewers for their constructive input which helped us to considerably improve our manuscript. We would further like to thank the German Space Operations Center (GSOC) of the German Aerospace Center (DLR) for providing continuously and nearly 100% of the raw telemetry data of the twin GRACE satellites. Moreover, we are grateful to C. Dahle and F. Flechtner (GFZ Potsdam) for providing the GRACE RL05a normal equations that allow us to account for GRACE

error characteristics and correlation patterns in our inverse method. In addition, we thank the GRACE processing centers for their continuous work with providing state of the art processed monthly GRACE gravity fields.

References

A, G., J. Wahr, and S. Zhong (2013), Computations of the viscoelastic response of a 3-D compressible Earth to surface loading: An application to Glacial Isostatic Adjustment in Antarctica and Canada, *Geophys. J. Int.*, *192*, 557–572, doi:10.1093/gji/ggs030.

Andersen, O., and R. Scharroo (2011), Range and Geophysical Corrections in Coastal Regions: And Implications for Mean Sea Surface Determination, pp. 103–104, Springer, doi:10.1007/978-3-642-12796-0.

Balmaseda, M. A., K. Mogensen, and A. T. Weaver (2013), Evaluation of the ECMWF ocean reanalysis system ORAS4, *Quarterly Journal of the Royal Meteorological Society*, *139*(674), 1132–1161, doi:10.1002/qj.2063.

Barletta, V. R., M. Bevis, B. E. Smith, T. Wilson, A. Brown, A. Bordoni, M. Willis, S. A. Khan, M. Rovira-Navarro, I. Dalziel, R. Smalley, E. Kendrick, S. Konfal, D. J. Caccamise, R. C. Aster, A. Nyblade, and D. A. Wiens (2018), Observed rapid bedrock uplift in Amundsen Sea Embayment promotes ice-sheet stability, *Science*, *360*(6395), 1335–1339, doi:10.1126/science.aao1447.

Boening, C., T. Lee, and V. Zlotnicki (2011), A record-high ocean bottom pressure in the South Pacific observed by GRACE, *Geophysical Research Letters*, *38*(4), doi:10.1029/2010GL046013.

Caron, L., E. R. Ivins, E. Larour, S. Adhikari, J. Nilsson, and G. Blewitt (2018), GIA Model Statistics for GRACE Hydrology, Cryosphere, and Ocean Science, *Geophysical Research Letters*, *45*(5), 2203–2212, doi:10.1002/2017GL076644.

Cazenave, A., K. Dominh, S. Guinehut, E. Berthier, W. Llovel, G. Ramillien, M. Ablain, and G. Larnicol (2009), Sea level budget over 2003–2008: A reevaluation from GRACE space gravimetry, satellite altimetry and Argo, *Global and Planetary Change*, *65*(1), 83–88, doi:10.1016/j.gloplacha.2008.10.004.

Chambers, D. P., and J. A. Bonin (2012), Evaluation of Release-05 GGRACE time-variable gravity coefficients over the ocean, *Ocean Science*, *8*, 859–868, doi:10.5194/os-8-859-2012.

Chambers, D. P., and J. K. Willis (2009), Low-frequency exchange of mass between ocean basins, *Journal of Geophysical Research: Oceans*, *114*(C11), doi:10.1029/2009JC005518.

Chambers, D. P., A. Cazenave, N. Champollion, H. Dieng, W. Llovel, R. Forsberg, K. von Schuckmann, and Y. Wada (2017), Evaluation of the Global Mean Sea Level Budget between 1993 and 2014, *Surveys in Geophysics*, *38*(1), 309–327, doi:10.1007/s10712-016-9381-3.

Chao, B. F. (2016), Caveats on the equivalent water thickness and surface mascon solutions derived from the GRACE satellite-observed time-variable gravity, *Journal of Geodesy*, *90*(9), 807–813, doi:10.1007/s00190-016-0912-y.

Chen, J. L., C. R. Wilson, and B. D. Tapley (2013), Contribution of ice sheet and mountain glacier melt to recent sea level rise, *Nature Geoscience*, *6*(7), 549–552, doi:10.1038/ngeo1829.

Cheng, M., B. D. Tapley, and J. C. Ries (2013), Deceleration in the Earth's oblateness, *Journal of Geophysical Research*, *118*, 1–8, doi:10.1002/jgrb.50058.

Church, J., P. Clark, A. Cazenave, J. Gregory, S. Jevrejeva, A. Levermann, M. Merrifield, G. Milne, R. Nerem, P. Nunn, A. Payne, W. Pfeffer, D. Stammer, and A. Unnikrishnan (2013), Climate Change 2013: The Physical Science Basis. Contribution of Working Group I to the Fifth Assessment Report of the Intergovernmental Panel on climate Change, pp. 1137–1216, Cambridge University Press, Cambride, United Kingdom and New York, NY, USA.

Dieng, H. B., H. Palanisamy, A. Cazenave, B. Meyssignac, and K. von Schuckmann (2015), The Sea Level Budget Since 2003: Inference on the Deep Ocean Heat Content, *Surveys in Geophysics*, *36*(2), 209–229, doi:10.1007/s10712-015-9314-6.

Dobslaw, H., F. Flechtner, I. Bergmann-Wolf, C. Dahle, R. Dill, S. Esselborn, I. Sasgen, and M. Thomas (2013), Simulating high-frequency atmosphere-ocean mmass variability for dealiasing of satellite gravity observations: AOD1B RL05, *Jornal of Geophysical Research: Oceans*, *118*, 3704–3711, doi:10.1002/jgrc.20271.

Döll, P., F. Kaspar, and B. Lehner (2003), A global hydrological model for deriving water availability indicators: Model tuning and validation, *Journal of Hydrology*, *270*(1), 105–134, doi:10.1016/S0022-1694(02)00283-4.

Douglas, B. C., and W. R. Peltier (2002), The Puzzle of Global Sea-Level Rise, *Physics Today*, *55*(3), 35–40, doi:10.1063/1.1472392.

Farrell, W. E., and J. A. Clark (1976), On Postglacial Sea Level, *Geophysical Journal of the Royal Astronomical Society*, *46*(3), 647–667, doi:10.1111/j.1365-246X.1976.tb01252.x.

Feng, W., and M. Zhong (2015), Global sea level variations from altimetry, GRACE and Argo data over 2005–2014, *Geodesy and Geodynamics*, *6*(4), 274–279, doi:10.1016/j.geog.2015.07.001.

Fenoglio-Marc, L., J. Kusche, and M. Becker (2006), Mass variation in the Mediterranean Sea from GRACE and its validation by altimetry, steric and hydrologic fields, *Geophysical Research Letters*, *33*(19), doi:10.1029/2006GL026851.

Flechtner, F., H. Dobslaw, and E. Fagiolini (2015), AOD1B Product Description Document for Product Release 05, *Tech. rep.*, GFZ German Research Centre for Geosciences, Department 1: Geodesy and Remote Sensing.

Flechtner, F., K.-H. Neumayer, C. Dahle, H. Dobslaw, E. Fagiolini, J.-C. Raimondo, and A. Güntner (2016), What Can be Expected from the GRACE-FO Laser Ranging Interferometer for Earth Science Applications?, *Surveys in Geophysics*, *37*(2), 453–470, doi:10.1007/s10712-015-9338-y.

Förstner, W. (1979), Ein Verfahren zur Schätzung von Varianz- und Kovarianzkomponenten, *Allgemeine Vermessungsnachrichten*, *86*(11–12), 446–453.

Jacob, T., J. Wahr, W. T. Pfeffer, and S. Swenson (2012), Recent contributions of glaciers and ice caps to sea level rise, *Nature*, *482*(7386), 514–518, doi:10.1038/nature10847.

Jensen, L., R. Rietbroek, and J. Kusche (2013), Land water contribution to sea level from GRACE and Jason-1measurements, *Journal of Geophysical Research: Oceans*, *118*(1), 212–226, doi:10.1002/jgrc.20058.

Johnson, G. C., and D. P. Chambers (2013), Ocean bottom pressure seasonal cycles and decadal trends from GRACE Release-05: Ocean circulation implications, *Journal of Geophysical Research: Oceans*, *118*(9), 4228–4240, doi:10.1002/jgrc.20307.

Kim, W., S.-W. Yeh, J.-H. Kim, J.-S. Kug, and M. Kwon (2011), The unique 2009–2010 El Niño event: A fast phase transition of warm pool El Niño to La Niña, *Geophysical Research Letters*, *38*(15), doi:10.1029/2011GL048521.

Klemann, V., and Z. Martinec (2009), Contribution of glacial-isostatic adjustment to the geocenter motion, *Tectonophysics*, *511*(3), 99–108, doi:10.1016/j.tecto.2009.08.031.

Klinger, B., and T. Mayer-Gürr (2016), The role of accelerometer data calibration within GRACE gravity field recovery: Results from ITSG-Grace2016, *Advances in Space Research*, *58*(9), 1597–1609, doi:10.1016/j.asr.2016.08.007.

Kusche, J. (2007), Approximate decorrelation and non-isotropic smoothing of time-variable GRACE-type gravity field models, *Journal of Geodesy*, *81*(11), 733–749, doi:10.1007/s00190-007-0143-3.

Kusche, J., B. Uebbing, R. Rietbroek, C. K. Shum, and Z. H. Khan (2016), Sea level budget in the Bay of Bengal (2002–2014) from GRACE and altimetry, *Journal of Geophysical Research: Oceans*, *121*(2), 1194–1217, doi:10.1002/2015JC011471.

Llovel, W., J. Willis, F. Landerer, and I. Fukumori (2014), Deep-ocean contribution to sea level and energy budget not detectable over the past decade, *Nature Climate Change*, *4*,

doi:10.1038/nclimate2387.

Lück, C., J. Kusche, R. Rietbroek, and A. Löcher (2018), Time-variable gravity fields and ocean mass change from 37 months of kinematic Swarm orbits, *Solid Earth*, *9*(2), 323–339, doi:https://doi.org/10.5194/se-9-323-2018.

Martín-Español, A., M. A. King, A. Zammit-Mangion, S. B. Andrews, P. Moore, and J. L. Bamber (2016), An assessment of forward and inverse GIA solutions for Antarctica, *Journal of Geophysical Research: Solid Earth*, *121*(9), 6947–6965, doi:10.1002/2016JB013154.

Mathers, E. L., and P. L. Woodworth (2006), A study of departures from the inverse-barometer response of sea level to air-pressure forcing at a period of 5 days, *Quarterly Journal of the Royal Meteorological Society*, *130*(597), 725–738, doi:10.1256/qj.03.46.

Müller Schmied, H., S. Eisner, D. Franz, M. Wattenbach, F. T. Portmann, M. Flörke, and P. Döll (2014), Sensitivity of simulated global-scale freshwater fluxes and storages to input data, hydrological model structure, human water use and calibration, *Hydrol. Earth Syst. Sci.*, *18*(9), 3511–3538, doi:10.5194/hess-18-3511-2014.

Nerem, R. S., D. P. Chambers, C. Choe, and G. T. Mitchum (2010), Estimating Mean Sea Level Change from the TOPEX and Jason Altimeter Missions, *Marine Geodesy*, *33*(sup1), 435–446, doi:10.1080/01490419.2010.491031.

Nerem, R. S., B. D. Beckley, J. T. Fasullo, B. D. Hamlington, D. Masters, and G. T. Mitchum (2018), Climate-change–driven accelerated sea-level rise detected in the altimeter era, *Proceedings of the National Academy of Sciences*, p. 201717312, doi:10.1073/pnas.1717312115.

Paulson, A., S. Zhong, and J. Wahr (2007), Inference of mantle viscosity from GRACE and relative sea level data, *Geophysical Journal International*, *171*(2), 497–508, doi:10.1111/j.1365-246X.2007.03556.x.

Peltier, W. R., D. F. Argus, and R. Drummond (2015), Space geodesy constrains ice age terminal deglaciation: The global ICE-6G_C (VM5a) model, *Journal of Geophysical Research: Solid Earth*, *120*(1), 450–487, doi:10.1002/2014JB011176.

Petrick, C., Dobslaw H., Bergmann-Wolf I., Schön N., Matthes K., and Thomas M. (2014), Low-frequency ocean bottom pressure variations in the North Pacific in response to time-variable surface winds, *Journal of Geophysical Research: Oceans*, *119*(8), 5190–5202, doi:10.1002/2013JC009635.

Piecuch, C. G., and K. J. Quinn (2016), El Niño, La Niña, and the global sea level budget, *Ocean Sci.*, *12*(6), 1165–1177, doi:10.5194/os-12-1165-2016.

Plag, H.-P., and H.-U. Juettner (2001), Inversion of global tide gauge data for present-day ice load changes (scientific paper), *Memoirs of National Institute of Polar Research. Special issue*, *54*, 301–317.

Ponte, R. M. (2006), Low-Frequency Sea Level Variability and the Inverted Barometer Effect, *Journal of Atmospheric and Oceanic Technology*, *23*(4), 619–629, doi:10.1175/JTECH1864.1.

Resplandy, L., R. F. Keeling, Y. Eddebbar, M. K. Brooks, R. Wang, L. Bopp, M. C. Long, J. P. Dunne, W. Koeve, and A. Oschlies (2018), Quantification of ocean heat uptake from changes in atmospheric O 2 and CO 2 composition, *Nature*, *563*(7729), 105, doi:10.1038/s41586-018-0651-8.

Rietbroek, R. (2014), Retrieval of Sea Level and Surface Loading Variations from Geodetic Observations and Model Simulations: An Integrated Approach, PhD Thesis, University of Bonn, Germany.

Rietbroek, R., S. E. Brunnabend, J. Kusche, and J. Schröter (2012), Resolving sea level contributions by identifying fingerprints in time-variable gravity and altimetry, *Journal of Geodynamics*, *59-60*, 72–81, doi:10.1016/j.jog.2011.06.007.

Rietbroek, R., S.-E. Brunnabend, J. Kusche, J. Schröter, and C. Dahle (2016), Revisiting the contemporary sea-level budget on global and regional scales, *Proceedings of the National Academy of Sciences*, *113*(6), 1504–1509, doi:10.1073/pnas.1519132113.

Scanlon, B. R., Z. Zhang, H. Save, A. Y. Sun, H. M. Schmied, L. P. H. van Beek, D. N. Wiese, Y. Wada, D. Long, R. C. Reedy, L. Longuevergne, P. Döll, and M. F. P. Bierkens (2018), Global models underestimate large decadal declining and rising water storage trends relative to GRACE satellite data, *Proceedings of the National Academy of Sciences*, p. 201704665, doi:10.1073/pnas.1704665115.

Scharroo, R., E. Leuliette, J. Lillibridge, D. Byrne, M. Naeije, and G. Mitchum (2013), RADS: Consistent Multi-Mission Products, in *20 Years of Progress in Radar Altimatry*, vol. 710, p. 69.

Sun, Y., P. Ditmar, and R. Riva (2016), Observed changes in the Earth's dynamic oblateness from GRACE data and geophysical models, *Journal of Geodesy*, *90*(1), 81–89, doi:10.1007/s00190-015-0852-y.

Sun, Y., P. Ditmar, and R. Riva (2017), Statistically optimal estimation of degree-1 and C20 coefficients based on GRACE data and an ocean bottom pressure model, *Geophysical Journal International*, *210*(3), 1305–1322, doi:10.1093/gji/ggx241.

Swenson, S., D. P. Chambers, and J. Wahr (2008), Estimating geocenter variations from a combination of GRACE and ocean model output, *Journal of Geophysical Research: Solid Earth*, *113*, doi:10.1029/2007JB005338.

Tamisiea, M. E. (2011), Ongoing glacial isostatic contributions to observations of sea level change, *Geophysical Journal International*, *186*(3), 1036–1044, doi:10.1111/j.1365-246X.2011.05116.x.

Thomas, M., J. Sündermann, and E. Maier-Reimer (2001), Consideration of ocean tides in an OGCM and impacts on subseasonal to decadal polar motion excitation, *Geophysical Research Letters*, *28*(12), 2457–2460, doi:10.1029/2000GL012234.

Timmermann, R., S. Danilov, J. Schröter, C. Böning, D. Sidorenko, and K. Rollenhagen (2009), Ocean circulation and sea ice distribution in a finite element global sea ice–ocean model, *Ocean Modelling*, *27*(3), 114–129, doi:10.1016/j.ocemod.2008.10.009.

van der Wal, W., P. L. Whitehouse, and E. J. O. Schrama (2015), Effect of GIA models with 3D composite mantle viscosity on GRACE mass balance estimates for Antarctica, *Earth and Planetary Science Letters*, *414*, 134–143, doi:10.1016/j.epsl.2015.01.001.

von Schuckmann, K., J.-B. Sallée, D. Chambers, P.-Y. Le Traon, C. Cabanes, F. Gaillard, S. Speich, and M. Hamon (2014), Consistency of the current global ocean observing systems from an Argo perspective, *Ocean Sci.*, *10*(3), 547–557, doi:10.5194/os-10-547-2014.

Wahr, J., R. S. Nerem, and S. V. Bettadpur (2015), The pole tide and its effect on GRACE time-variable gravity measurements: Implications for estimates of surface mass variations, *Journal of Geophysical Research: Solid Earth*, *120*(6), 4597–4615, doi:10.1002/2015JB011986.

WCRP-Global-Sea-Level-Budget-Group (2018), Global sea-level budget 1993–present, *Earth System Science Data*, *10*(3), 1551–1590, doi:https://doi.org/10.5194/essd-10-1551-2018.

Whitehouse, P. L., M. J. Bentley, G. A. Milne, M. A. King, and I. D. Thomas (2012), A new glacial isostatic adjustment model for Antarctica: Calibrated and tested using observations of relative sea-level change and present-day uplift rates, *Geophysical Journal International*, *190*(3), 1464–1482, doi:10.1111/j.1365-246X.2012.05557.x.

Wu, X., J. Kusche, and F. W. Landerer (2017), A new unified approach to determine geocentre motion using space geodetic and GRACE gravity data, *Geophysical Journal International*, *209*(3), 1398–1402, doi:10.1093/gji/ggx086.

Zuo, H., M. A. Balmaseda, and K. Mogensen (2017), The new eddy-permitting ORAP5 ocean reanalysis: Description, evaluation and uncertainties in climate signals, *Climate Dynamics*, *49*(3), 791–811, doi:10.1007/s00382-015-2675-1.

Supporting Information for "Processing choices affect ocean mass estimates from GRACE"

B. Uebbing[1], **J. Kusche**[1], **R. Rietbroek**[1], **F. W. Landerer**[2]

[1]Institute of Geodesy and Geoinformation, University of Bonn, D-53115 Bonn, Germany
[2]Jet Propulsion Laboratory, California Institute of Technology, Pasadena, CA 91109, USA

Contents

Corresponding author: Bernd Uebbing, uebbing@geod.uni-bonn.de

S1: Applied Corrections in the Direct and Inverse Method

Table 1. Overview over the applied corrections for the direct and inverse approaches for deriving ocean mass time series. Here JC13 refers to the direct method following [Johnson and Chambers, 2013] while R16 refers to the inverse method described in [Rietbroek et al., 2016] and R16E to the extension explained in the main manuscript.

		JC13	R16	R16E
GRACE	Weighting individual months	uniform	full covariance matrix	full covariance matrix
	Degree-1	external data	estimated	estimated
	c_{20}	external data	estimated	estimated
	mean field	2005–2010	EIGEN-6C3	EIGEN-6C3
	Wahr et al. [2015] pole tide	no	no	yes
	GIA correction	*A et al.* [2013]	estimating 5 scaling factors to external model	prescribed to *A et al.* [2013]
	Spatial smoothing	no	no	no
	Leakage correction	none	hydrology patterns	hydrology patterns
	Restoring AOD1B	GAD[a]	GAC ocean mean	GAD[b]
altimetry	weighting	-	uniform	uniform
	altimetry correction	-	estimating altimeter biases	estimating altimeter biases
	steric correction	-	estimating EOF scales	estimating EOF scales
OBP	patterns for inversion	-[c]	in residual patterns	OBP patterns

[a] This refers to the GAD correction using the monthly full ocean mean to correct for the IB effect, as well as using the 300km Buffer basin.

[b] This refers only to the GAD correction using the monthly full ocean mean to correct for the IB effect.

[c] The OBP signal is included in the GRACE data and consequently in the ocean mass estimate.

S2: Ocean Mask

Below we provide the ocean mask used in this study. In addition we show results obtained with two additional slightly modified 300km ocean masks and the effect on GRACE direct solutions for degree and order 40 and 60 (Table 2). As discussed in Section 3.4 in the main manuscript, the degree and order 40 estimates appear to be more robust with respect to the choice of ocean mask compared to the degree and order 60 solutions.

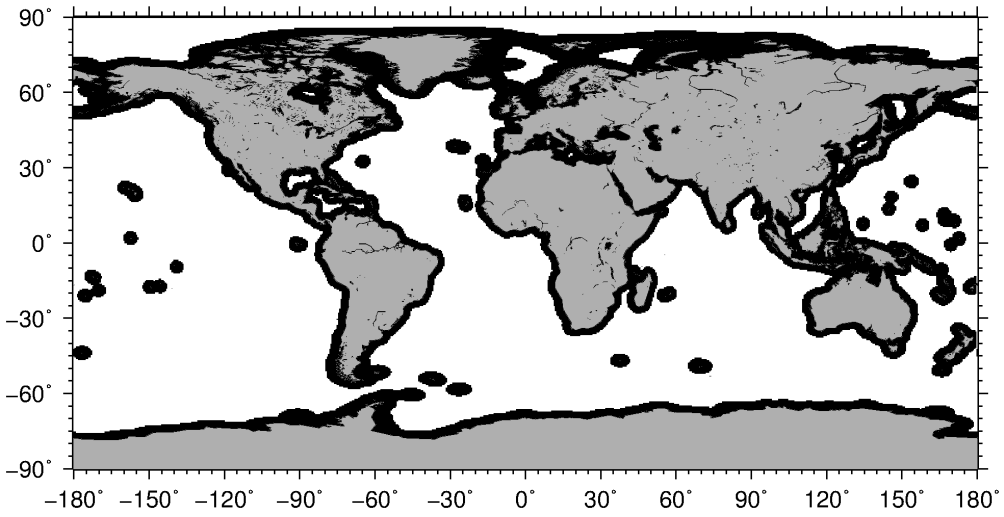

Figure 1. Ocean mask applied in this study. In addition a coastal buffer zone of 300km is shown in black.

Table 2. Global OMC trends [mm/y] (2002.6 – 2014.5) for reconstructing the downloaded time series based on JC13. Mask1 = used in this study (derived using GMT), Mask 2 = provided by JPL (derived from 1 deg grid) and Mask 3 = mask from this study which has been manually edited to be more similar to mask in Fig. 2 from Johnson and Chambers (2013)

	CSR d/o 40 $[\frac{mm}{y}]$	**CSR d/o 60** $[\frac{mm}{y}]$	**GFZ d/o 40** $[\frac{mm}{y}]$	**GFZ d/o 60** $[\frac{mm}{y}]$
Mask 1	1.829	1.749	1.772	1.721
Mask 2	1.847	1.843	1.804	1.888
Mask 3	1.843	1.805	1.765	1.749
JC13 (downloaded)	–	1.812	–	1.747

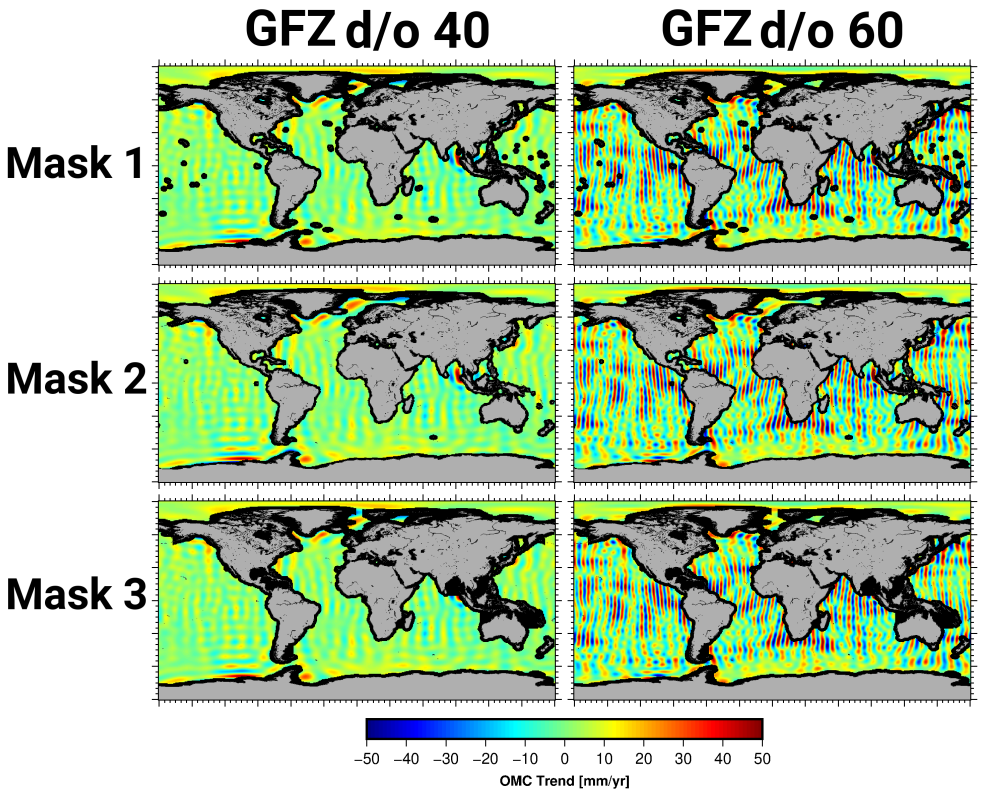

Figure 2. GRACE GFZ-RL05a OMC trendmaps (2002.6 – 2014.5) for d/o 40 and d/o 60 for 3 different masks. Mask1 = is used in this study (derived using GMT), Mask 2 = provided by JPL (derived from 1 deg grid) and Mask 3 = mask from this study which has been manually edited to be more similar to mask in Fig. 2 from Johnson and Chambers (2013)

S3: Application of a 500km Coastal Buffer Zone

Table 3. Ocean mass trends derived from the direct and inverse methods. All trends are computed as mean over the full ocean minus a 500 km buffer zone along the coasts. See also Fig 1. No additional smoothing has been applied. For the GAD correction, 0km/500km refers to utilizing a 0km/500km bufferzone ocean basin for computing the ocean mean GAD see Eq. (4) in the main manuscript. All trends are provided in equivalent water height (EWH). $\Delta\text{GIA}^{\textit{Rietbroek et al.}\ [2016]}_{\textit{A et al.}\ [2013]}$ describes the difference between the GIA trends from *Rietbroek et al.* [2016] and *A et al.* [2013].

Source	2002.6-2014.5 $[\frac{mm}{y}]$	2005.0-2013.9 $[\frac{mm}{y}]$	2002.6-2016.5 $[\frac{mm}{y}]$
Own proc. *Johnson and Chambers* [2013] (500 km GAD) CSR	1.666	1.893	2.010
Own proc. *Johnson and Chambers* [2013] (500 km GAD) GFZ	1.580	1.855	1.896
same but 0 km GAD, CSR	1.314	1.543	1.674
same but 0 km GAD, GFZ	1.256	1.530	1.586
same but 0 km GAD + *Wahr et al.* [2015] pole tide, CSR	1.192	1.410	1.547
same but 0 km GAD + *Wahr et al.* [2015] pole tide, GFZ	1.229	1.503	1.560
Own proc. 0 km GAD, CSR, deg-1 + GIA *Rietbroek et al.* [2016]	0.717	0.953	-
Own proc. 0 km GAD, GFZ, deg-1 + GIA *Rietbroek et al.* [2016]	0.658	0.942	-
Rietbroek et al. [2016]	0.805	1.079	-
Rietbroek et al. [2016] + $\Delta\text{GIA}^{\textit{Rietbroek et al.}\ [2016]}_{\textit{A et al.}\ [2013]}$	1.390	1.664	-
Inversion, with 0km GAD, *A et al.* [2013] GIA and *Wahr et al.* [2015] pole tide	1.466	1.784	-
GIA *A et al.* [2013]		-1.027	
GIA *Rietbroek et al.* [2016]		-0.442	
OMCT degree 1-40 CSR	-0.445	-0.445	-0.437

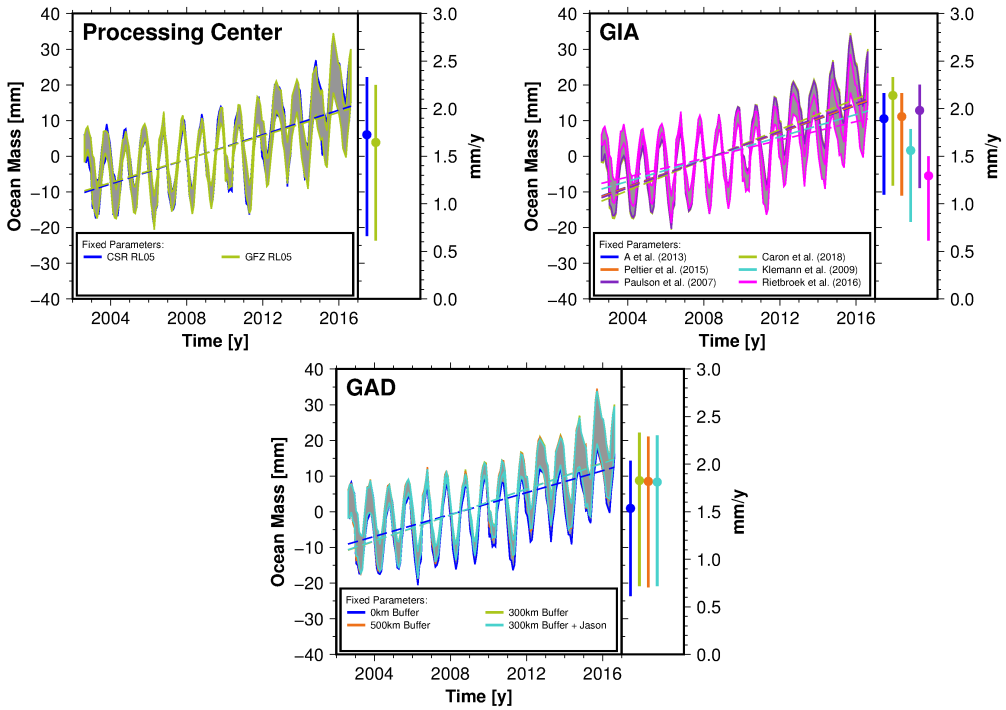

Figure 3. Ensembles per processing choice discussed in this study. The indicated processing option is kept fixed while all other possible combinations of the remaining three processing options form the corresponding ensemble. The right part of the plot shows the minimum, maximum and median trends extracted from the time series of the corresponding sub-ensemble. The option "300km Buffer + Jason" refers to additionally limiting the mask to areas between ±66° which is covered by the Jason missions.

S4: Inversion Method

The inverse method [*Jensen et al.*, 2013; *Rietbroek et al.*, 2012; *Kusche et al.*, 2016; *Rietbroek et al.*, 2016] allows to separate the total sea level change into contributions due to the melting of the ice-sheets in Greenland and Antarctica, melting of land glaciers, variations in terrestrial hydrology and steric (volumetric) sea level change. The individual contributions are parameterized by a set of forward modeled, global, normalized and temporally invariant spatial patterns, usually termed 'fingerprints'. We then fit the 429 fingerprints to a combination of GRACE gravity and satellite altimetry data and estimate monthly scaling factors for each of the individual fingerprints. Here, we provide an overview over the main steps of the fingerprint inversion and indicate where changes have been made with respect to the consistent inversion run in this study. Detailed description of the individual processing steps can be found in *Rietbroek et al.* [2012], *Jensen et al.* [2013], *Rietbroek* [2014] and *Rietbroek et al.* [2016].

Mass Fingerprints

For the *Rietbroek et al.* [2016], mass contributions are discretized by 119 global fingerprints, of which 27 and 16 relate to basins in Antarctica and Greenland, 16 to major glacier clusters (from WGI/GLIMS database, Raup et al., 2007), and 60 to land water storage change (2002–2010) derived from the WGHM model [*Döll et al.*, 2003]. Each individual mass fingerprint represent a passive ocean response derived utilizing the Sea Level Equation [*Farrell and Clark*, 1976]. This equation relates load mass change δh at location λ', θ' to changes in sea level $\delta s(\lambda, \theta, t)$

$$\begin{aligned}\delta s(\lambda,\theta,t) =& O(\lambda,\theta)\int_{\Omega} G^{L}_{N-U}(\delta s(\lambda',\theta',t) + dh(\lambda',\theta',t))d\omega \\ &+ \int_{\Omega} G^{T}_{N-U}\delta\Lambda(\delta s,\delta h)d\omega + \frac{\Delta V}{g}.\end{aligned}$$

The sea level equation accounts for self-gravitation as well as the effect of the changing rotational potential $\delta\Lambda$ (rotational feedback): The Green's functions G^{L}_{N-U} and G^{T}_{N-U} model the elastic response of the Earth to loading (L) and potential forcing (T), in terms of geoid change N with respect to the elastically uplifting/subsiding ocean bottom and land surface U. In the equation above, $O(\lambda, \theta)$ represents the ocean function. In order to conserve mass, $\frac{\Delta V}{g}$ allows for a uniform shift with respect to the geoid. The numerical approach that we employ to solve the Sea Level Equation in the spectral domain is described in detail in *Rietbroek et al.* [2012] and *Rietbroek* [2014].

Modifying the Treatment of the Ocean Bottom Pressure Signal

For the inversion run, which is as consistent as possible with the direct approach utilized in this study, we have added 10 additional mass patterns related to ocean bottom pressure (OBP) changes which are derived from the ORAP5 ocean model [*Zuo et al.*, 2017]. For the *Rietbroek et al.* [2016] inversion all computations have been done with the AOD1B background GAC model removed from, both, the GRACE and the altimetry data (see also Section 3.2 in the main manuscript). This also effectively removed the modeled OBP from the data. However, to be consistent with the direct approach, we now restore the GAD model as described in Eq. (3) in the main manuscript. We have restored the complete time-variable OBP signal to the GRACE data, which requires the parameterization by the OBP patterns.

We apply a principal component analysis to the modeled OBP data and utilize the 10 most dominant empirical orthogonal functions (EOFs) which cover the majority of the total variance as additional fingerprints. We constrain the derived OBP-fingerprints to have a zero mean and trend over the ocean by removing the average over the total ocean from

the monthly data before computing the EOFs. This way the fingerprints represent the internal mass variations within the ocean.

Steric Fingerprints

For the computation of the steric fingerprints, we utilize the Finite Element and Sea-ice Ocean Model (FESOM) [*Timmermann et al.*, 2009]. The modeled variations in temperature and salinity over a depth range from the sea surface down to the sea-floor have been converted to anomalies of steric sea level change. We apply a principal component analysis on the steric data (1990–2011) and extract the leading 200 EOFs covering more than 99% of the variance. These represent the steric fingerprints used in the inversion approach. We chose such a high number of steric fingerprints in order to sufficiently model the high spatial and temporal variation of the steric component.

GIA Fingerprints

For the *Rietbroek et al.* [2016] inversion, five additional fingerprints related to glacial isostatic adjustment are fitted. Instead of completely relying on a given a-priori model, this allows to fit changes to the a-priori model related to the major former glaciated regions, i.e. Laurentide, Antarctica, Greenland, Fernoscandia and a set of complementary glacial sources. The patterns have been kindly provided to us by V. Klemann for separate (ICE5G) mass load histories and VM2-2 rheology. The GIA is estimated as a linear trend over the total time period for each of the five regions. Consequently, the a-priori model (here: [*Klemann and Martinec*, 2009]) is removed before the estimation and only the differences to the a-priori model are fitted.

Enforcing a GIA Correction in the Inversion

For the inversion run that is as consistent as possible with the direct approach, we substituted the a-priori model with the one from *A et al.* [2013] and did not estimate any differences for the major GIA regions, i.e. we fixed the corresponding parameters to zero.

Augmented Patterns by Assessing Altimetry Residuals

After a first run of the inversion, the sum of all modeled components does not agree perfectly with the altimetry data. Therefore, we derive an additional set of fingerprints from the residuals with altimetry under the assumption that the residuals still include a significant signal which could not be modeled by the mass and steric fingerprints. We termed these patterns 'other' to indicate that these include other, non-modeled effects. These can be remaining steric effects due to the high spatial and temporal variability of the steric component, wind related effects, internal mass redistributions, etc. However since the mass time series from the direct and inverse approach agree well (see main manuscript) we assume that the majority of the signal contained in these 'other'-patterns is not related to mass changes.

We grid the residuals with altimetry utilize the 100 leading EOFs derived from a principal component analysis as a set of additional fingerprints for a second iteration of the inversion.

Input Data

In order to separate the total sea level change into individual mass and steric contributions, we utilize GRACE gravity data and satellite altimetry data.

GRACE Data

The GRACE mission observes the ocean mass changes directly. It is blind with respect to observing steric changes as these represent volume or density changes while the overall mass remains constant. Consequently, the GRACE data can only be fitted to the mass components of the inversion approach. The GRACE input data consists of full, unsolved and unfiltered monthly GFZ RL05 GRACE normal equation (NEQ) systems complete up to degree and order 150. These are transformed to lie in the lower dimensional space spanned by the fingerprints. In case the individual NEQ systems are solved directly up to degree and order 90, one would derive the same level–2 spherical harmonic coefficients that are provided to the community as monthly potential coefficients. Directly utilizing and transforming the NEQs allows us to incorporate the covariance information into our estimations, which would not be possible from the publicly available level–2 product.

The observation equation for the GRACE stokes coefficients is given by:

$$\delta C_{nm}(t) = \mathbf{D} \begin{bmatrix} \mathbf{x}_{mass}(t) \\ (t - t_0)\mathbf{x}_{gia} \end{bmatrix} + \epsilon$$

Here, the matrix $\mathbf{D}$ includes the mass fingerprints developed into spherical harmonic coefficients and $\mathbf{x}_{mass}(t)$ and $\mathbf{x}_{gia}$ contain the monthly estimated scaling factors for each individual mass and GIA related fingerprint. ϵ is the corresponding error. The subscripts "n" and "m" refer to the degree and order of the spherical harmonic expansion, respectively. For the consistent inversion run proposed in this study, the design matrix $\mathbf{D}$ additionally contains the fingerprints related to OBP and, consequently, the parameter vector $\mathbf{x}_{mass}(t)$ its corresponding scaling factors.

Altimetry Data

Satellite altimetry observes the total sea level change, i.e. the sum of the steric and mass component. Consequently, the altimetry data is fitted to the mass, as well as the steric component of the inversion in order to separate the mass changes which are also observed by the GRACE mission from the steric sea level change. The altimetry data employed in the inversion is 1Hz Jason-1 and Jason-2 along-track sea level anomaly (SLA) data extracted from the Radar Altimetry Database System (RADS) [*Scharroo et al.*, 2013]. The relation between a 1Hz SLA measurement $\delta h_{SLA}(t)$ and our fingerprints is given by:

$$\delta h_{SLA}(t) = \mathbf{YB} \begin{bmatrix} \mathbf{x}_{mass}(t) \\ \mathbf{x}_{gia} \end{bmatrix} + \mathbf{KC} \begin{bmatrix} \mathbf{x}_{steric}(t) \\ \mathbf{x}_{other}(t) \end{bmatrix} + \mathbf{P}[\mathbf{x}_{satbias}] + \epsilon$$

The matrix $\mathbf{B}$ contains the mass fingerprints expressed in geocentric sea level and the matrix $\mathbf{Y}$ maps the spherical harmonic coefficients in $\mathbf{B}$ to each individual altimetry measurement position. The scaling coefficients $\mathbf{x}_{mass}(t)$ and $\mathbf{x}_{gia}$ are the same as in the observation equation for the GRACE data. The gridded steric and 'other' (residual) fingerprints are contained in the matrix $\mathbf{C}$ are interpolated to the altimetry positions by the bilinear interpolation matrix $\mathbf{K}$. The steric and 'other' parameters are given by $\mathbf{x}_{steric}(t)$ and $\mathbf{x}_{other}(t)$, respectively. Although, the RADS data are already corrected for a constant offset between the individual altimetry missions we additionally fit a constant offset vector (given by $\mathbf{P}[\mathbf{x}_{satbias}]$) for each altimetry mission to correct some remaining small offsets. Again, ϵ represents the error.

Least Squares Inversion

From the observation equations above, it is possible to derive NEQ systems for each satellite mission (GRACE, Jason-1 and Jason-2). The monthly NEQ system is given in the form of

$$\mathbf{N}_{mission}(t)\mathbf{x}(t) = \mathbf{b}_{mission}(t)$$

Here, $\mathbf{N}_{mission}(t)$ is the normal equation matrix for each satellite mission and $\mathbf{b}_{mission}(t)$ the corresponding right hand side. The vector $\mathbf{x}(t)$ contains all monthly scaling factors to be estimated (see observations equations above).

The monthly normal equation systems from each satellite mission are then combined to a single system by utilizing the addition theorem for normal equations, as well as variance component estimation [*Förstner*, 1979]. For details on these steps, please see *Rietbroek et al.* [2012], *Rietbroek* [2014] and *Rietbroek et al.* [2016].

Reconstruction of Sea Level Change

After the monthly parameters $\mathbf{x}(t)$ have been estimated, it is possible to reconstruct the sea level changes related to individual patterns by multiplying each fingerprint with its corresponding monthly scaling factors. Similarly the sea level contribution for groups of patterns (e.g. Greenland or the sum of all mass patterns) can be derived by summing over the corresponding individual contributions for each month.

References

A, G., J. Wahr, and S. Zhong (2013), Computations of the viscoelastic response of a 3-D compressible Earth to surface loading: An application to Glacial Isostatic Adjustment in Antarctica and Canada, *Geophys. J. Int.*, *192*, 557–572, doi:10.1093/gji/ggs030.

Döll, P., F. Kaspar, and B. Lehner (2003), A global hydrological model for deriving water availability indicators: Model tuning and validation, *Journal of Hydrology*, *270*(1), 105–134, doi:10.1016/S0022-1694(02)00283-4.

Farrell, W. E., and J. A. Clark (1976), On Postglacial Sea Level, *Geophysical Journal of the Royal Astronomical Society*, *46*(3), 647–667, doi:10.1111/j.1365-246X.1976.tb01252.x.

Förstner, W. (1979), Ein Verfahren zur Schätzung von Varianz- und Kovarianzkomponenten, *Allgemeine Vermessungsnachrichten*, *86*(11–12), 446–453.

Jensen, L., R. Rietbroek, and J. Kusche (2013), Land water contribution to sea level from GRACE and Jason-1measurements, *Journal of Geophysical Research: Oceans*, *118*(1), 212–226, doi:10.1002/jgrc.20058.

Johnson, G. C., and D. P. Chambers (2013), Ocean bottom pressure seasonal cycles and decadal trends from GRACE Release-05: Ocean circulation implications, *Journal of Geophysical Research: Oceans*, *118*(9), 4228–4240, doi:10.1002/jgrc.20307.

Klemann, V., and Z. Martinec (2009), Contribution of glacial-isostatic adjustment to the geocenter motion, *Tectonophysics*, *511*(3), 99–108, doi:10.1016/j.tecto.2009.08.031.

Kusche, J., B. Uebbing, R. Rietbroek, C. K. Shum, and Z. H. Khan (2016), Sea level budget in the Bay of Bengal (2002–2014) from GRACE and altimetry, *Journal of Geophysical Research: Oceans*, *121*(2), 1194–1217, doi:10.1002/2015JC011471.

Rietbroek, R. (2014), Retrieval of Sea Level and Surface Loading Variations from Geodetic Observations and Model Simulations: An Integrated Approach, PhD Thesis, University of Bonn, Germany.

Rietbroek, R., S. E. Brunnabend, J. Kusche, and J. Schröter (2012), Resolving sea level contributions by identifying fingerprints in time-variable gravity and altimetry, *Journal of Geodynamics*, *59-60*, 72–81, doi:10.1016/j.jog.2011.06.007.

Rietbroek, R., S.-E. Brunnabend, J. Kusche, J. Schröter, and C. Dahle (2016), Revisiting the contemporary sea-level budget on global and regional scales, *Proceedings of the National Academy of Sciences*, *113*(6), 1504–1509, doi:10.1073/pnas.1519132113.

Scharroo, R., E. Leuliette, J. Lillibridge, D. Byrne, M. Naeije, and G. Mitchum (2013), RADS: Consistent Multi-Mission Products, p. 69.

Timmermann, R., S. Danilov, J. Schröter, C. Böning, D. Sidorenko, and K. Rollenhagen (2009), Ocean circulation and sea ice distribution in a finite element global sea ice–ocean model, *Ocean Modelling*, *27*(3), 114–129, doi:10.1016/j.ocemod.2008.10.009.

Wahr, J., R. S. Nerem, and S. V. Bettadpur (2015), The pole tide and its effect on GRACE time-variable gravity measurements: Implications for estimates of surface mass variations, *Journal of Geophysical Research: Solid Earth*, *120*(6), 4597–4615, doi:10.1002/2015JB011986.

Zuo, H., M. A. Balmaseda, and K. Mogensen (2017), The new eddy-permitting ORAP5 ocean reanalysis: Description, evaluation and uncertainties in climate signals, *Climate Dynamics*, *49*(3), 791–811, doi:10.1007/s00382-015-2675-1.